Serine Racemase is a Cysteine Racemase and Physiologic Down Regulator of Insulin Promoter Methylation

Robin Roychaudhuri[1], Moataz M. Gadalla[3], Lauren Albacarys[1], Timothy West[1], Harry Saavedra[4], Mario Amzel[4] and Solomon H. Snyder[1,2,3]***

Affiliations:

[1] Department of Neuroscience, Johns Hopkins University School of Medicine, Baltimore, MD 21205, USA

[2] Department of Psychiatry and Behavioral Sciences, Johns Hopkins University School of Medicine, Baltimore, MD 21287, USA

[3] Department of Pharmacology and Molecular Sciences, Johns Hopkins University School of Medicine, Baltimore, MD 21287, USA

[4]Department of Biological Chemistry, Johns Hopkins University School of Medicine, Baltimore, MD 21287, USA

Contact info:

** Corresponding author and lead contact: robinroychaudhuri@gmail.com

*Co corresponding author: ssnyder@jhmi.edu.

Abstract. Endogenous D-stereoisomers are being recognized as functionally important molecules in mammals. Here we report the first identification of endogenous D-cysteine in mammalian pancreas. Serine Racemase (SR) is the biosynthetic enzyme for D-cysteine. D-cysteine is present in substantial amounts in the eyes, brain and pancreas of mice. To characterize endogenous D-cysteine, we used SR deficient mice lacking racemizing ability and show 3.5 fold reduction in pancreatic D-cysteine. $SR^{-/-}$ mice produce 6-10 fold higher levels of insulin in the pancreas and plasma and are stored as amyloid aggregates in secretory vesicles and exosomes respectively. Lack of SR and endogenous D-cysteine globally decreased levels of nucleotides and cAMP, followed by reduced phosphorylation of CREB (S133) including lower expression of DNA methyltransferase (DNMT) 1, 3A and 3B, and reduced DNMT enzymatic and promoter activities in the pancreas. This results in decreased DNA methylation globally and specifically of the *Ins1* promoter. D-cysteine is efficiently metabolized by D-amino acid oxidase and transported by ASCT2 and Asc1 transporters in cells. Dietary supplementation with methyl donors rescues the high insulin levels and low DNMT activity in $SR^{-/-}$ mice. Our data show that SR racemizes cysteine in the pancreas and is a physiologic down regulator of insulin promoter methylation.

Keywords. D-cysteine, serine racemase, insulin promoter methylation, cAMP, functional amyloid, methyl donor diet, Asc1, ASCT2, DNMT1, CREB.

Introduction.

D-amino acids are mirror images of L-amino acids which occur in mammals, but their functions are unclear (Corrigan, 1969) (Genchi, 2017, Lehmann & Ye, 2019). Most work on D-amino acids have been restricted to prokaryotes and lower eukaryotes. Cloning of serine racemase (SR) from mouse brain (Wolosker, Blackshaw et al., 1999a, Wolosker, Sheth et al., 1999b), as well as the presence of substantial levels of D-amino acids in mammals in the different organs points to physiologic roles (Fuchs, Berger et al., 2005, Tsai, Yang et al., 2006). D-serine and D-aspartate are the two major stereoisomers whose roles have been well studied as ligands at the NMDA receptor (Basu, Tsai et al., 2009, Kim, Duan et al., 2010). They appear to play roles in neuronal development, functioning as novel neurotransmitters (Snyder, 2017, Snyder & Ferris, 2000). While much of the work has focused on D-serine and D-aspartate, little is known about endogenous D-cysteine in mammals (Roychaudhuri & Snyder, 2022, Semenza, Harraz et al., 2021). Here, we report the presence of endogenous D-cysteine in the pancreas of mice and elucidate its function.

D-cysteine is synthesized by SR in a pyridoxal phosphate (PLP) dependent racemization reaction from L-cysteine. SR has higher affinity for L-cysteine than L-serine. Mice deficient in SR ($SR^{-/-}$) produce 6-10 fold higher levels of insulin in both the pancreas and plasma. $SR^{-/-}$ mice are hypoglycemic and have 3 fold higher mean islet diameters. The excess insulin in these mice is stored in secretory vesicles and plasma exosomes as functional amyloid. $SR^{-/-}$ mice produce higher levels of glycogen and the ketone bodies 3-OH butyrate and 2-OH butyrate in the liver. Endogenous D-cysteine controls nucleotide metabolism and signals via a cAMP dependent mechanism. $SR^{-/-}$

mice show lower levels of CREB and p-CREB (S133) and total DNMT activity, which results in lower levels of global and *Ins1* promoter methylation.

Using biochemical methods followed by *Ins1* promoter bisulfite sequencing and global mass spectrometric approaches, we identify endogenous D-cysteine and the role of its biosynthetic enzyme SR in the pancreas. Other D-stereoisomers may also have potentially novel roles in mammalian biology.

Results.

Identification and characterization of mammalian D-cysteine.

We employed biochemical and chromatographic methods to estimate D-cysteine in the pancreas. SR is a PLP dependent enzyme that racemizes L-serine to D-serine and *vice versa* (Raboni, Marchetti et al., 2018, Wolosker et al., 1999a, Wolosker et al., 1999b). Using a bioluminescent luciferase assay [13], (Bailey, Donor et al., 2015), (Niwa, Nakamura et al., 2006) to measure D-cysteine (**Fig. 1A**), we estimated its levels in the pancreas of WT and $SR^{-/-}$ mice (Basu et al., 2009). The luciferase assay is specific to D-cysteine as it involves the conjugation of cyano hydroxy benzothiazole (CHBT) with D-cysteine in presence of TCEP and base to form D-luciferin, which serves as an exclusive substrate in the presence of ATP for firefly luciferase to produce bioluminescence (**Fig. 1B** adapted from Niwa et al) (Bailey et al., 2015, Corrigan, 1969, Niwa et al., 2006, Semenza et al., 2021). This forms the basis of the stereospecific detection of D-cysteine. The bioluminescence emitted is directly proportional to the amount of D-cysteine present (**Fig. S1A**). The assay was specific for D-cysteine (**Fig. S1B**). We generated standard curves of D-cysteine in rabbit pancreatic lysates (to

eliminate contribution from endogenous L-cysteine) and in other mice organs and found strong correlation of bioluminescence with concentration of exogenously added D-cysteine (**Fig S1A**). WT pancreas contained 35 μM while $SR^{-/-}$ mice contained 10 μM D-cysteine (**Fig. 1C**). We estimated D-cysteine levels in βTC-6 insulin secreting cell line with or without lentiviral knockdown of SR (SR#8) (**Fig. S2A**). Knock down of SR in βTC-6 cells elicited two fold reduction in D-cysteine levels (**Fig. S2B).** These results indicate that SR is the biosynthetic enzyme for D-cysteine.

In addition to the pancreas, D-cysteine was also present in mouse and human brain(Roychaudhuri & Snyder, 2022, Semenza et al., 2021) and in the outer nuclear layer of the eyes at significantly higher amounts (100 μM) compared to the pancreas of 6 weeks old mice (**Fig. S3A-B**). The levels of D-cysteine in the eye increase more than 5 fold from 6 weeks to 12 months (**Fig. S3C**). We also estimated D-cysteine levels in the pancreas using chiral HPLC following thiol labeling with ABD-F (4-(aminosulfonyl)-7-fluoro-2, 1, 3-benzoxadiazole) and fluorescent detection (Hiratsuka, 1993, Toyo'oka, 1984) (**Fig. 1D**). HPLC estimation showed four fold molar excess of L-cysteine in the pancreas relative to D-cysteine with D-cysteine level at approximately 30 μM in WT and 10 μM in $SR^{-/-}$ mouse pancreas (**Fig. 1E**).

To further evaluate SR as a biosynthetic enzyme for D-cysteine, we used the luciferase assay to determine racemization of 1 mM L-cysteine to D-cysteine by purified recombinant mouse SR in the presence of Mg^{2+} and PLP. Purified mouse SR efficiently racemizes L-cysteine to D-cysteine with time (**Fig. 1F**). Interestingly, high concentrations of L-cysteine competitively inhibit SR (Dunlop & Neidle, 2005). We used 500 mM L-cysteine as a saturating concentration of substrate in absence of PLP as a

negative control. This was done to provide enough substrate for catalysis and also eliminate any substrate regulatory effects of L-cysteine. Negative control showed no activity over time (**Fig. 1F**).

We next determined the localization of D-cysteine in mouse pancreas using a monoclonal antibody towards conjugated D-cysteine. D-cysteine staining was predominantly observed in the islets with sparse staining observed in the exocrine pancreas (**Fig. 1G**) (**Fig. S9A**) (Lockridge, Baumann et al., 2016). Lack of staining in $SR^{-/-}$ pancreas confirmed that SR was the source of D-cysteine (**Fig. 1G**). Colocalization studies in pancreas of with a β-cell marker insulin and D-cysteine, showed D-cysteine to be present mainly in β-cells (**Fig. 1H**). To correlate D-cysteine levels in the pancreas with SR, we determined expression of SR in both endocrine and exocrine pancreas. We found higher expression of SR in the islets compared to exocrine pancreas (**Fig. S9B**) (Lockridge et al., 2016).

Spontaneous *in vitro* racemization rates of different amino acids indicate cysteine with the shortest racemization $t_{1/2}$ of 2 days compared to serine ($t_{1/2}$ =3 days) and aspartate ($t_{1/2}$ = 30 days) (Man & Bada, 1987). To determine if L-serine or L-cysteine is the preferred substrate for SR, we assessed kinetics of racemization by purified recombinant mouse SR using the amplex red assay to measure peroxide generated from breakdown of D-cysteine generated during L-serine racemization (Nelson, Applegate et al., 2017, Tomoko Naka, 2010). Our kinetic data showed that L-cysteine had a K_m of 0.0173 mM compared to 0.0412 mM for L-serine (**Table 1**). This suggests that L-cysteine has a higher affinity for SR during racemization than L-serine. Evidence for L-cysteine being a better (higher affinity) substrate than L-serine is also seen from

racemization inhibition studies performed with 10 mM L and D cysteine (as inhibitors) that led to >95% inhibition of L-serine racemization. Cysteine was the only amino acid whose L and D enantiomers both inhibit serine racemization consistent with cysteine also being a substrate for SR (Panizzutti, De Miranda et al., 2001). Interestingly, SR is inhibited (only lower V_{max}) at higher concentrations of L-cysteine (>1mM) suggesting that it serves as a substrate for SR and that endogenous D-cysteine maybe under strict regulatory control *in vivo* (Dunlop & Neidle, 2005).

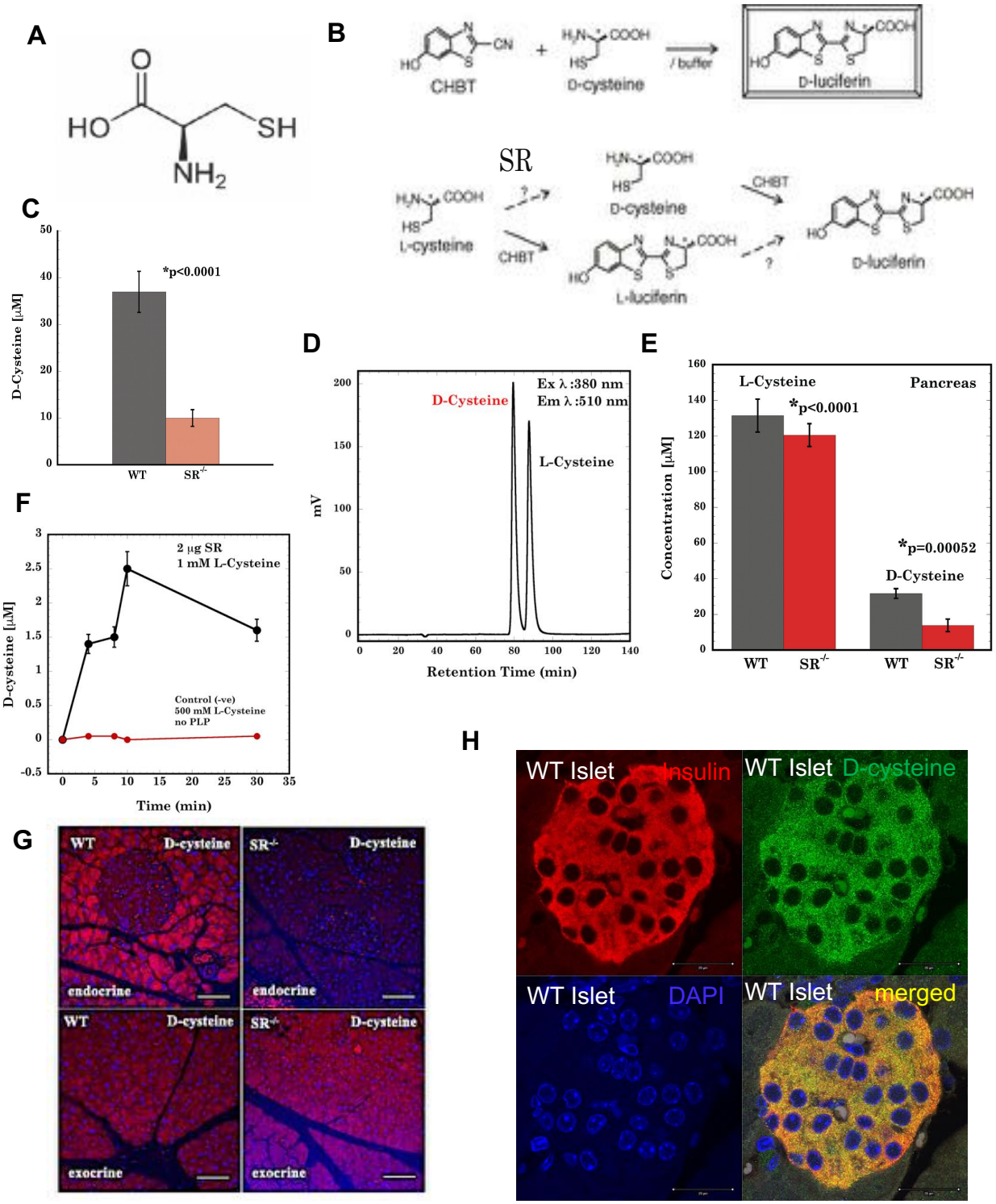

Figure. 1

Figure. 1. Identification and characterization of mammalian D-cysteine.

SR controls insulin secretion and islet size.

$SR^{-/-}$ mice displayed a four fold reduction of D-cysteine in the pancreas (**Fig. 1C**) and produced significantly higher levels of insulin in both pancreas and plasma (fed state) (**Figs. 2A, 2B**). Plasma insulin levels also measured during fasting (t=16h) show significantly elevated insulin levels in age matched $SR^{-/-}$ mice (**Fig. S8A**). These mice also contained high levels of glycogen in the liver (**Fig. 2C**) (Rasouli, Ostovar-Ravari et al., 2014). $SR^{-/-}$ mice also produced higher levels of the ketone bodies 2-hydroxybuyrate and 3-hydroxybutyrate in the liver (**Table 2**) suggesting that under hypoglycemia, ketone bodies could serve as a significant circulating energy source (Newman & Verdin, 2014, Puchalska & Crawford, 2017, Saleem, Ametaj et al., 2012). $SR^{-/-}$ mice displayed 3 fold larger mean islet diameters and 4 fold higher total β-cell area compared to age matched control mice (**Figs. 2D, 2E, 2F and S10**). In tests of glucose tolerance, $SR^{-/-}$ mice displayed a trend towards increased glucose metabolism with time (**Fig. 2G**). During the GTT, $SR^{-/-}$ mice also displayed significantly higher levels of insulin compared to WT mice (**Fig. 2H**). To determine if the high insulin levels reflect abnormal transport and or processing, we measured gene expression of pre and mature pancreatic insulin. Our results (**Fig. 2I**) showed more than 10 fold increase in mRNA levels of both pre and mature forms of insulin in the pancreas of $SR^{-/-}$ mice. Interestingly, glucagon, the counter hormone to insulin showed no change in mRNA. To determine if genes related to glucose transport, islet development and insulin processing were affected by D-cysteine, we determined expression of key genes (**Figs. 2K, 2L and 2M**) revealing a trend towards significant upregulation in $SR^{-/-}$ mice pancreas. Nkx6.1, a major

transcription factor in pancreatic development was also significantly upregulated (**Fig. 2J**) (Taylor, Liu et al., 2013).

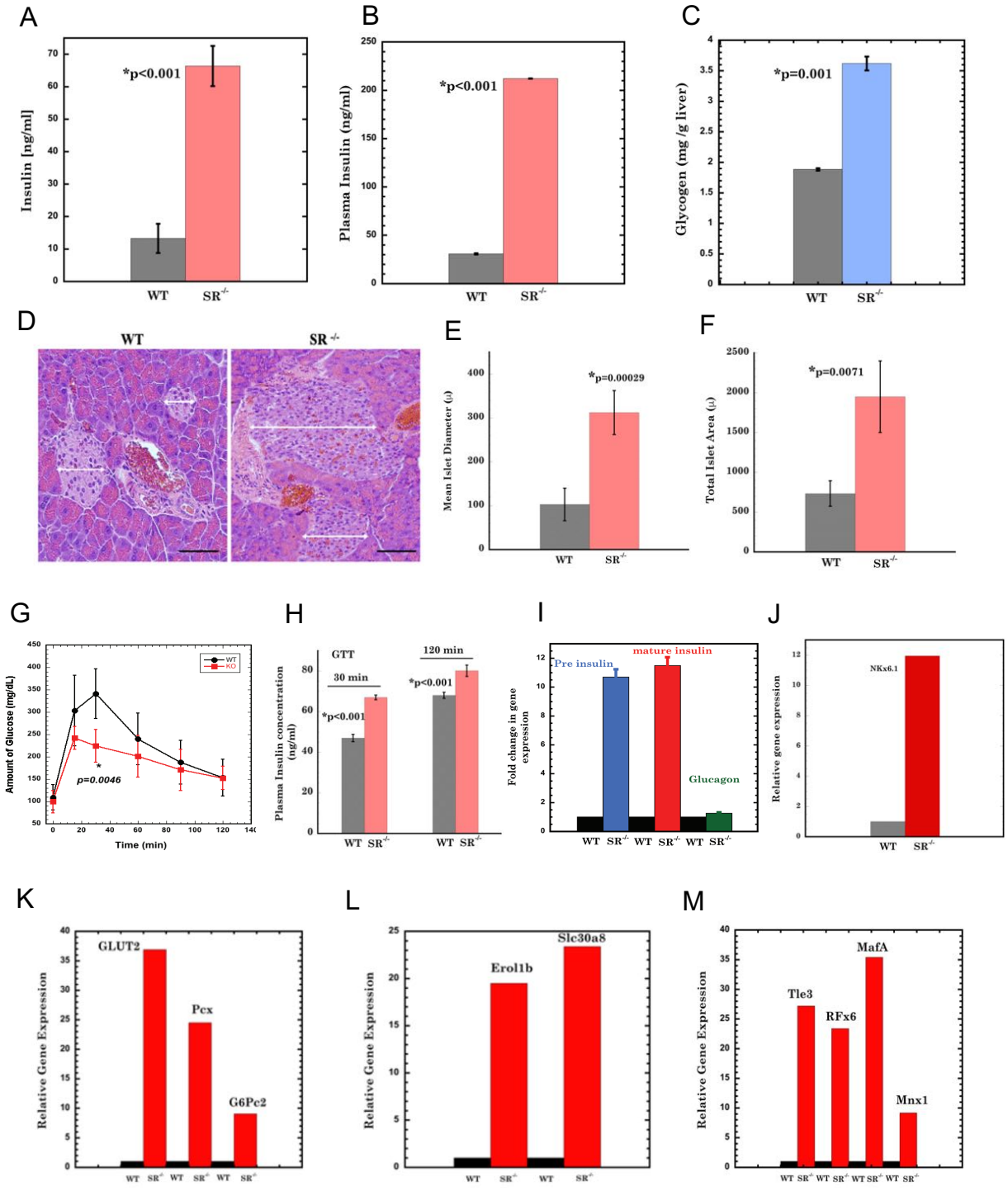

Figure. 2

Figure. 2. SR controls insulin secretion and islet size.

Excess insulin is stored as functional amyloid in secretory vesicles and exosomes.

SR$^{-/-}$ mice are fertile, healthy, have a normal lifespan and produce healthy offspring. We investigated the tolerance of SR$^{-/-}$ mice to constitutively elevated levels of insulin in the pancreas and plasma. A prior study had shown that secretory hormones like insulin, glucagon and parathyroid hormones are stored in specialized secretory vesicles as functional amyloids, as a mode of regulation (Maji, Perrin et al., 2009).

We isolated secretory vesicles from pancreas of WT and SR$^{-/-}$ mice by differential gradient ultracentrifugation (Hutton, Wong et al., 2009) and assayed insulin containing fractions using dot blot assays. Secretory vesicles from pancreas of SR$^{-/-}$ mice contained higher amounts of amyloid aggregates compared to age matched WT control mice (**Fig. 3A**). To determine if these aggregates comprised insulin, we double immunostained pancreatic sections from WT and SR$^{-/-}$ mice for amyloid (generic OC antibody for fibrillar aggregates) (Bigi, Loffredo et al., 2020, Kayed, Head et al., 2007, Krishnan, Goodman et al., 2012, Maji et al., 2009) and insulin. Our data show increased expression and strong colocalization of amyloid aggregates and insulin in the islets of SR$^{-/-}$ mice (**Fig. 3B**). Thioflavin-S, a dye used for staining amyloid aggregates was also used to visualize amyloid deposits in the islets (Reinke & Gestwicki, 2011, Wei, Wu et al., 2005). Our results show greater Thioflavin-S staining in islets of SR$^{-/-}$ mice indicative of β-sheet aggregates of amyloid (**Fig. 3I**). We performed similar experiments in secretory vesicles from β-TC6 cells. Dot blot assays in WT and SR#8 βTC-6 cells

showed higher expression of insulin in SR#8 cells (**Fig. 3C**) compared to WT and also increased expression of amyloid aggregates in the secretory vesicles of SR#8 βTC-6 cells (**Fig. 3E**). Colocalization of amyloid and insulin in βTC-6 cells showed a similar trend. SR#8 βTC-6 cells showed higher expression of colocalized insulin and amyloid aggregates (**Fig. S4**). Since plasma of $SR^{-/-}$ mice also showed high levels of insulin, we isolated exosomes from plasma and assayed the size and the presence of β-sheet amyloid aggregates following lysis. Electron micrographic analysis showed that plasma exosomes from $SR^{-/-}$ mice were larger compared to WT (**Figs. 3D, 3F**). To determine if these exosomes contained β-sheet aggregates, we performed a Thioflavin T (ThT) assay time course to ascertain protein assembly following lysis of exosomes and secretory vesicles. ThT is a dye that intercalates between β-sheet aggregates to produce fluorescence (Biancalana & Koide, 2010, Roychaudhuri, Lomakin et al., 2014). Our results with mouse plasma exosomes (**Fig. 3G**) and βTC-6 secretory vesicles showed that $SR^{-/-}$ exosomes and SR#8 vesicles produced significantly enhanced ThT fluorescence indicating the presence of higher amounts of β-sheet aggregates (**Fig. 3H**). These data suggest that the high levels of insulin in $SR^{-/-}$ mice and in SR#8 βTC-6 cells are stored as amyloid aggregates in the exosomes and secretory vesicles, allowing the mice to remain healthy, viable and fertile.

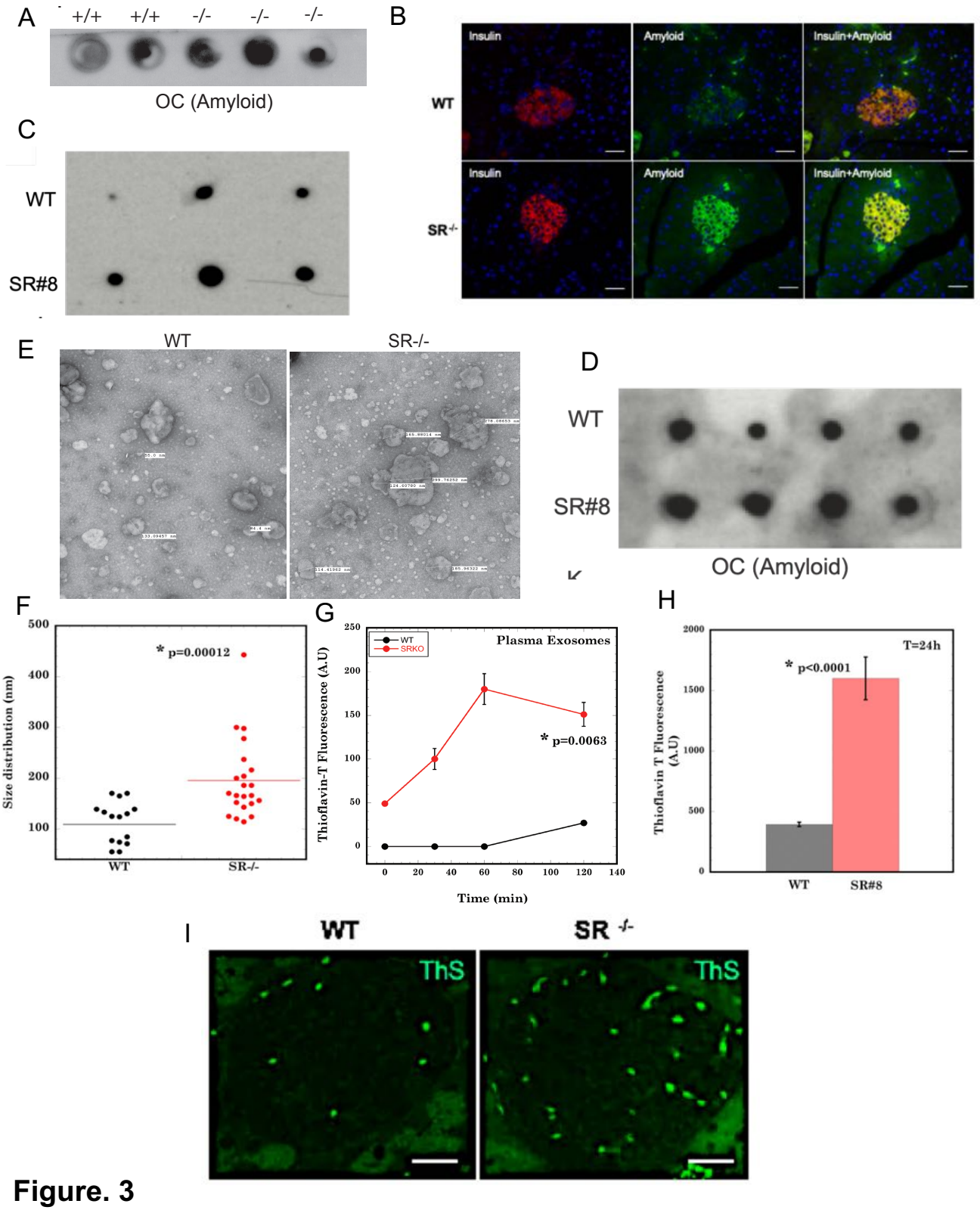

Figure. 3

Figure. 3. Excess insulin is stored as functional amyloid in secretory vesicles and exosomes.

D-cysteine is efficiently degraded by D-amino acid oxidase.

D-amino acid oxidase (DAO) is a flavin adenine nucleotide (FAD) dependent enzyme that regulates the physiological concentrations of various D-stereoisomers in vivo (Khoronenkova & Tishkov, 2008, Pollegioni, Sacchi et al., 2018, Yamanaka, Miyoshi et al., 2012). To determine if D-cysteine serves as a substrate for DAO, we performed in vitro kinetic assays with purified porcine DAO towards D-serine and D-cysteine, measuring the production of L-glutamate from ammonia and α-ketoglutarate by glutamate dehydrogenase in presence of NADPH (Sasamura, Matsuda et al., 2002). Since DAO is a peroxisomal enzyme, it is assayed at the physiological pH of peroxisomes (pH 7.0-7.5) where the thiol group of cysteine is not readily oxidized (Jankowski, Kim et al., 2001). Most DAO assays rely on the detection of hydrogen peroxide. However, this is unsuitable when cysteine is the substrate as the free thiol on cysteine can react with hydrogen peroxide to quench the signal. D-serine is a well-known substrate for DAO (Pollegioni et al., 2018). Our kinetics data show that porcine DAO can degrade D-cysteine equally efficiently as D-serine. In vitro kinetics of purified porcine DAO showed a K_m of 225 μM for both D-cysteine and D-serine and V_{max} of 0.002 μmoles/min for D-cysteine and V_{max} of 0.0019 μmoles/min for D-serine. These data suggest that D-cysteine and D-serine are equally efficient DAO substrates with similar affinities (**Table 3**). Competition assays monitoring the degradation of D-cysteine by DAO using the luciferase assay showed that adding equimolar amounts of D-serine

did not affect the degradation of D-cysteine suggesting that D-cysteine may be equally efficient or even a better substrate than D-serine (Bailey et al., 2015).

SR controls nucleotide metabolism in the pancreas.

To determine the function of D-cysteine in the pancreas and identify D-cysteine interacting proteins, we performed label free quantitative mass spectrometry (nano LC-MS/MS) in pancreatic lysates of age matched WT and $SR^{-/-}$ mice (Bian, Zheng et al., 2020). The MS screen identified a total of 555 proteins. Analysis of data showed upregulation (>3 fold change relative to WT) of proteins related to fatty acid, glucose and protein metabolism (**Fig. 4A** and **Table 4**). Notable increase in expression (relative to WT) were observed in islet regenerating factor, cellular transport, ribosomal protein synthesis, ubiquitination and chaperone proteins. Notable decreases (>2 fold or higher than WT, **Fig. S5**) were observed in proteins involved in actin cytoskeleton assembly, folate biosynthesis, mitochondrial electron transfer, pancreatic lipid hydrolysis and serpin2. Interestingly, we observed a 5 fold decrease in cytosolic 10-formyl tetrahydrofolate dehydrogenase which is involved in mitochondrial 1C metabolism and controls S-adenosyl methionine (SAM) levels (Anguera, Field et al., 2006).

Serine metabolism derived ribose, one carbon units and cysteine synthesis are synergistically integrated into the methionine cycle through *de novo* ATP synthesis which fuels the generation of SAM. To determine upstream action of D-cysteine, we performed an unbiased nucleotide screen of pancreatic lysates of WT and $SR^{-/-}$ mice by Ultra Performance Liquid Chromatography-Multiple Reaction Monitoring/Mass Spectrometry (UPLC-MRM-MS). The results of the screen revealed significant

reduction in levels of different mono, di and tri nucleotides namely AMP, ADP, GMP, GDP, GTP, dGTP, IMP, dIMP IDP, CTP, TTP and TMP (**Figs. 4B-M, S7**).

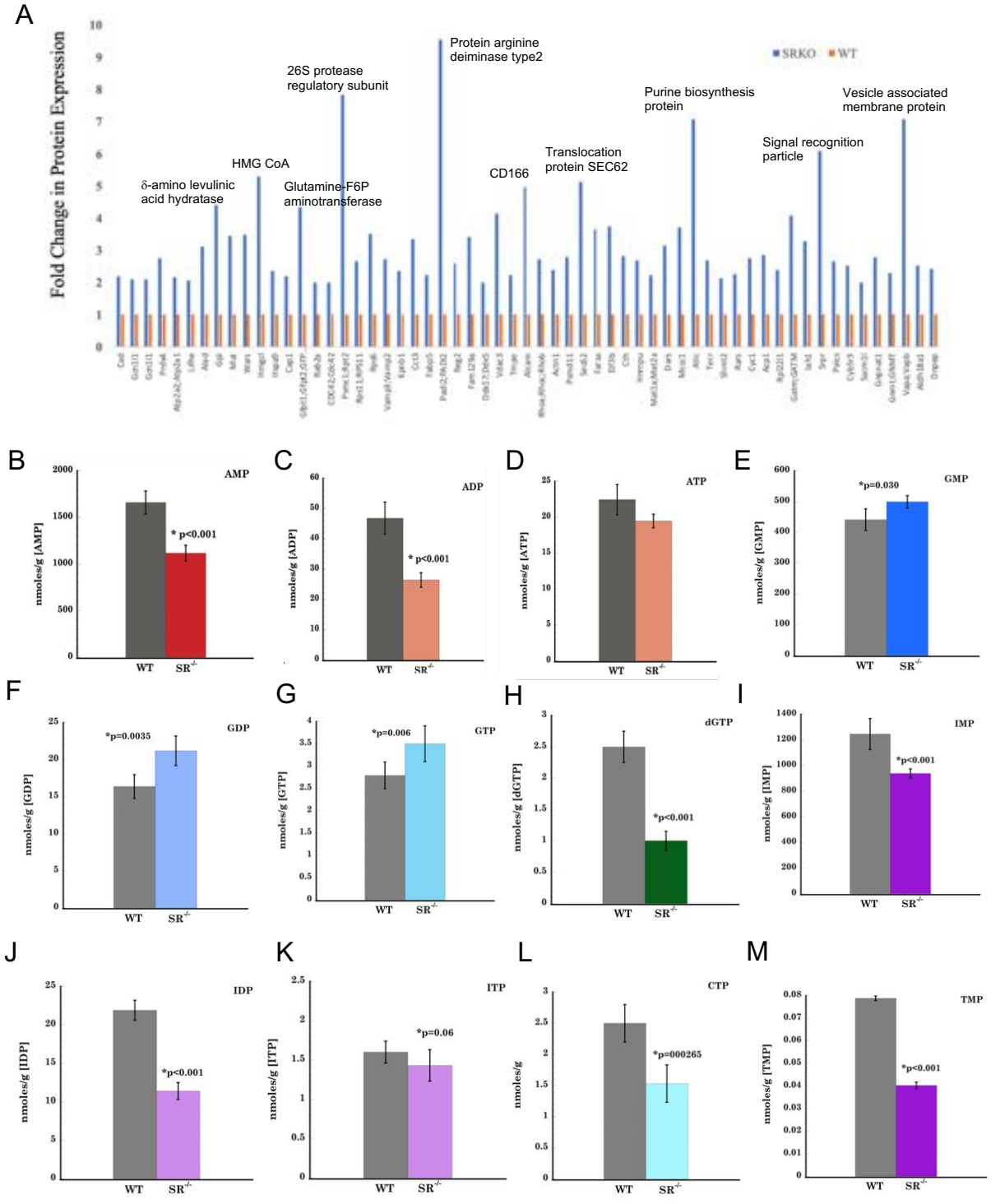

Figure. 4

Figure. 4. SR controls nucleotide metabolism in the pancreas.

D-Cysteine signals via a cyclic AMP dependent mechanism

To determine if the global decrease in nucleotide levels affect the most common second messenger cyclic AMP (cAMP), we performed quantitative ELISA using a cAMP standard curve. Our data show significantly lower levels of cAMP (*p<0.0001 relative to WT) in the pancreas of $SR^{-/-}$ mice compared to age matched controls (**Fig. 5A**). To further investigate if D-cysteine signals via cAMP, we performed live cell imaging in βTC-6 cells transfected with the cAMP sensor Pink Flamindo (Pink Fluorescent cAMP indicator) (Harada, Ito et al., 2017) and treated with equimolar amounts of L-cysteine, D-cysteine and forskolin (50 μM concentration each). Snapshot of time points from live cell imaging (**Movies S1-S4**) by spinning idisk confocal microscopy and quantitative estimation of a snapshot during the live cell imaging show that D-cysteine treatment in βTC-6 cells produced maximal fluorescence (562 nm) among the different treatment groups (**Figs. 5C**, **5D**). To determine if stimulation of cAMP production by D-cysteine was specific to βTC-6 cells, we performed an identical experiment using HEK293 cells. Results from HEK293 cells show that D-cysteine treatment results in higher cAMP fluorescence at 562 nm that is comparable to forskolin (positive control), and reduced in cells treated with L-cysteine or vehicle (**Fig. S6**). To determine tissue distribution of cAMP and confirm our live cell imaging, we performed immunohistochemistry on pancreatic sections from age matched WT and $SR^{-/-}$ mice and observed diminished levels of cAMP in both exocrine and islet regions of $SR^{-/-}$ mice relative to control (**Fig. 5B**). Our data from different experimental formats show that D-cysteine signals via cAMP (**Fig. 5E**).

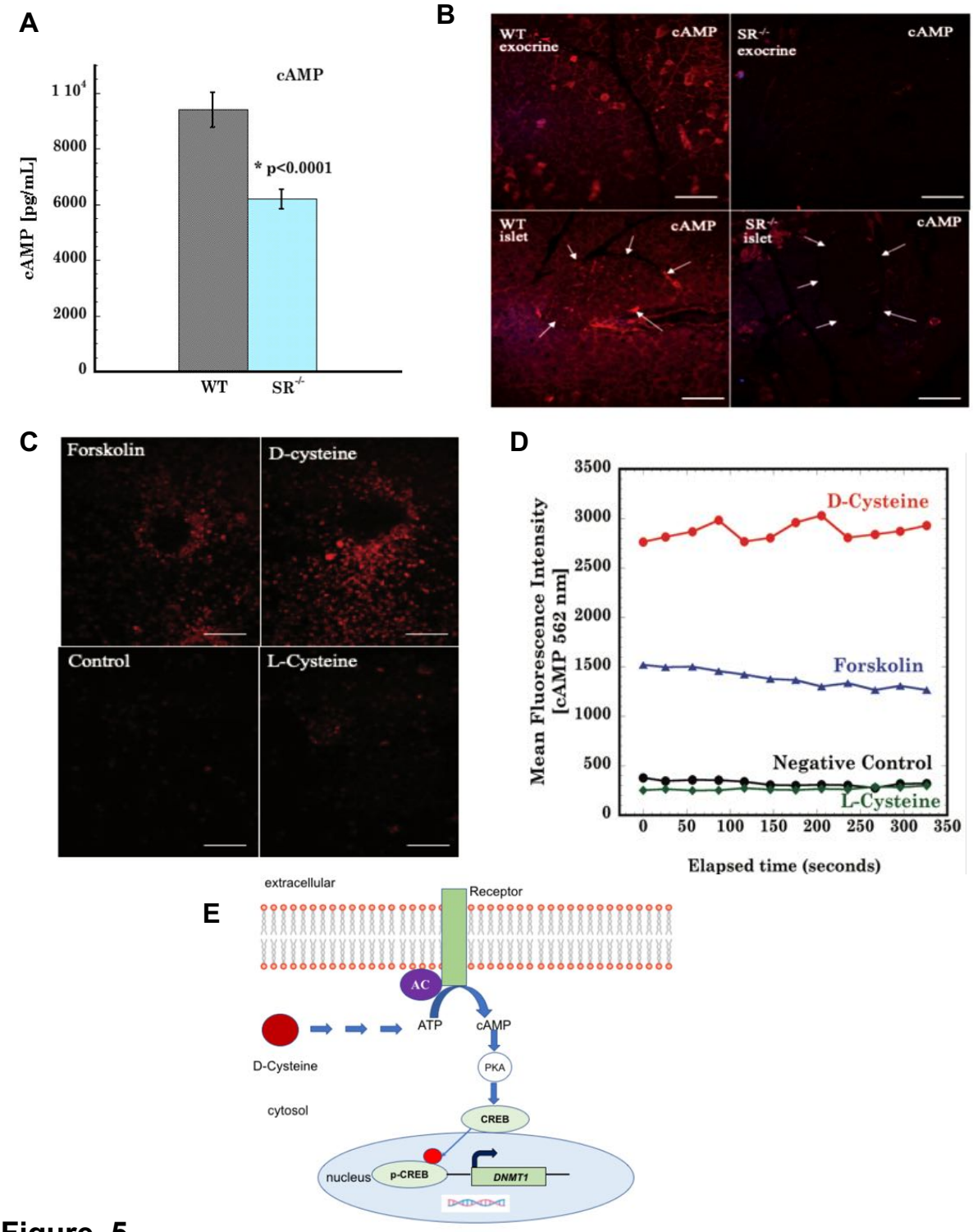

Figure. 5

Figure. 5. D-Cysteine signals via cAMP dependent mechanism.

SR controls global and *Ins1* promoter methylation.

To determine a mechanistic basis for the high levels of insulin in the plasma and pancreas of $SR^{-/-}$ mice, we examined an epigenetic mode of regulation. Our rationale was based on the five-fold reduction of cytosolic enzyme 10-formyl tetrahydrofolate dehydrogenase in a global pancreatic proteomics screen. This enzyme controls S-adenosyl methionine (SAM) levels in the cell and DNA methylation.

To evaluate methylation of the *Ins1*promoter, we performed bisulfite sequencing around the 2500 bp position containing CpG islands (**Fig. 6C**) (Gao, Liang et al., 2015, Lister, Pelizzola et al., 2009, Olova, Krueger et al., 2018). Our data showed lower levels of methylation at positions 33, 60, 113, 133, 147 and 156 of the *Ins1* promoter of $SR^{-/-}$ pancreas with the most difference (compared to WT) seen at positions 33, 113 and 133 indicated by *p* values (**Fig. 6F**). These data suggest that lower levels of methylation of the *Ins*1 promoter may lead to high levels of insulin expression in $SR^{-/-}$ mice. We also determined global levels of methyl cytosine (mC) and hydroxymethyl cytosine (hmC) modifications in pancreatic DNA. DNA dot blot assays from pooled N=12-15 mice per group showed lower levels of mC (**Fig. 6D**) and hmC (**Fig. 6E**) in $SR^{-/-}$ mice, implying global downregulation of DNA methylation.

CREB is a transcription factor that controls *DNMT1* gene expression (Impey, McCorkle et al., 2004). To further elaborate a mechanism, we measured expression of CREB and phospho CREB in pancreatic lysates and nuclear extracts. We observed lower levels of total CREB and phospho-CREB (S133) in pancreatic lysates (**Fig. 6A**) and in nuclear extracts (**Fig. 6B**).

To elaborate a mechanistic basis for the decrease in global and specifically *Ins1* promoter methylation in $SR^{-/-}$ mice, we first determined the expression of major DNMT enzymes in nuclear extracts of pancreas. Expression of DNMT1, DNMT3A and DNMT3B were significantly reduced in $SR^{-/-}$ mice (**Fig. 6G**). We also estimated total DNMT activity in nuclear extracts of pancreas from WT and $SR^{-/-}$ mice. Our results show that $SR^{-/-}$ mice displayed approximately 80 % reduction in total DNMT activity compared to WT (**Fig. 6I**).

To determine if lower levels of CREB affect *DNMT1* promoter activity, we performed chromatin immunoprecipitation with a CREB antibody followed by real time PCR (ChIP-qPCR). We divided the *DNMT1* promoter into 5 regions (D1-D5) spanning bp from -1149 to 183 (**Fig. 6H**) (Zampieri, Passananti et al., 2009). To determine promoter enrichment, we determined the fold change in CREB binding in regions D1-D5 in WT and $SR^{-/-}$ immunoprecipitated DNA against an input control DNA. We detected significant reduction in CREB binding to the *DNMT1* promoter in all regions except D3 (**Fig. 6J**) in $SR^{-/-}$ DNA. The greatest differences were observed in regions D1, D2 and D5. These results suggest that CREB is a transcription factor controlling *DNMT1* expression, and that lower levels of total CREB in $SR^{-/-}$ pancreas results in lower expression of *DNMT1* gene and decreased levels of methylation of the different gene promoters and specifically of the *Ins1* promoter.

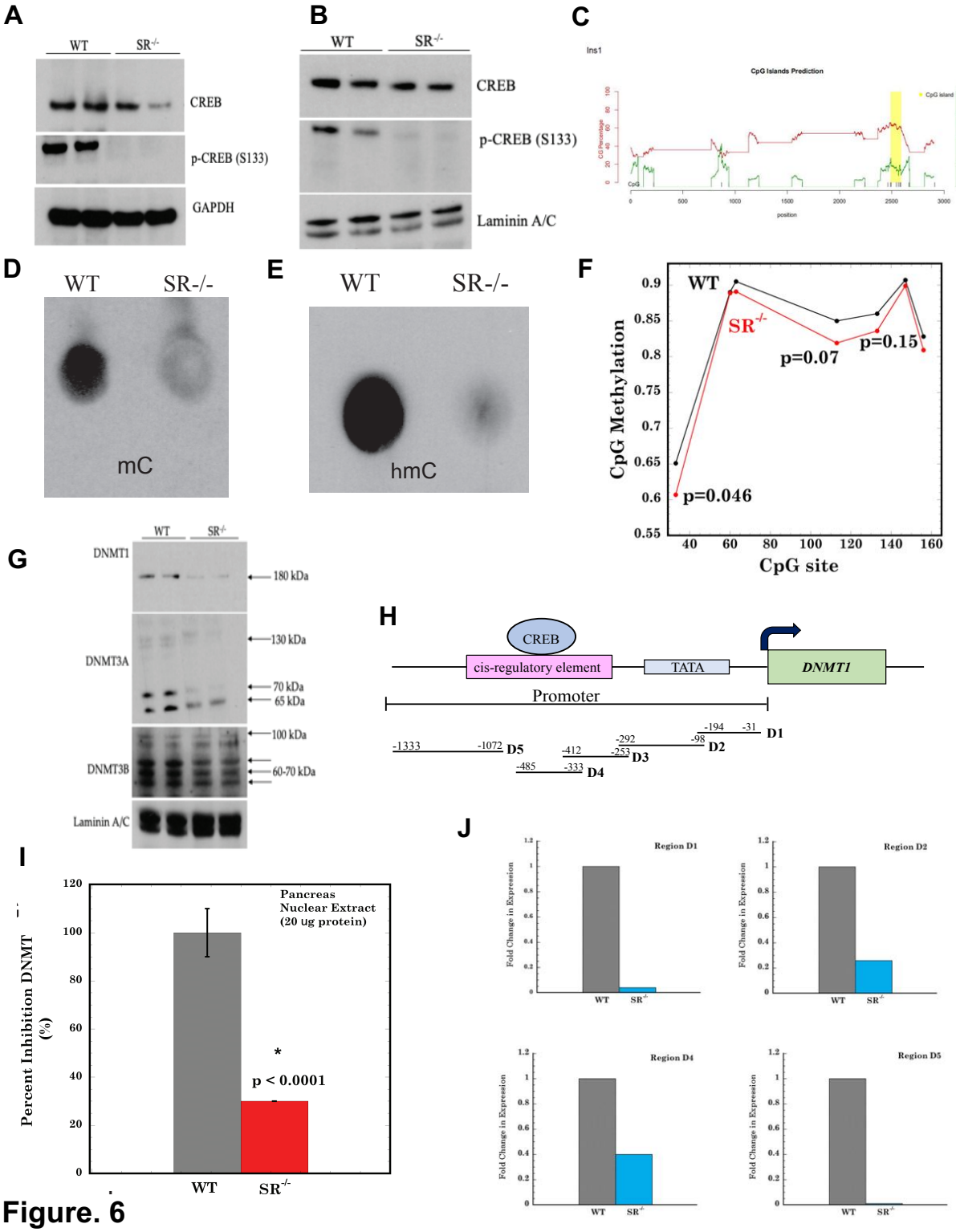

Figure. 6

Figure. 6. SR controls global and *Ins1* promoter methylation.

Methyl donor dietary supplementation rescues excess insulin secretion and DNMT activity.

Methionine in the diet serves as a precursor for SAM, S-adenosyl homocysteine (SAH) and 1 carbon metabolism in the liver. SAM is synthesized by the methionine cycle from multiple precursors like folate, choline, betaine and methionine. The ratio of SAM to SAH, called the methylation index, is indicative of DNA methylation (**Fig. 7A**) (Anguera et al., 2006, Zhang, 2015). To determine if the high levels of insulin in $SR^{-/-}$ mice could be rescued to physiological levels by providing methionine (substrate for methylating machinery), we fed WT and $SR^{-/-}$ mice a high carbohydrate diet containing 0.8 % methionine and or a normal diet containing 0.4 % methionine for 6 months (*ad libitum*). $SR^{-/-}$ mice fed a normal diet produced 3 fold higher levels of insulin compared to control mice. $SR^{-/-}$ mice fed a high carb diet containing 0.8 % methionine had significantly reduced levels of insulin compared to $SR^{-/-}$ mice fed a normal diet (**Fig. 7B**). $SR^{-/-}$ mice fed a normal diet had higher body weights (not obese) compared to age matched WT mice (**Fig. S8C**). Plasma insulin levels (**Fig. 7D**) also showed approximately 8 fold reduction in insulin levels in $SR^{-/-}$ mice fed a diet high in methionine compared to the same mice fed normal diet. DNA dot blot from the 6 months dietary supplementation experiment showed partial rescue with higher levels of global mC and hmC in mice fed a higher methionine diet (**Fig. 7C**).

To determine if the rescue in insulin levels was due to methionine in the high carbohydrate diet, we fed age matched WT and $SR^{-/-}$ mice an exclusive methyl donor supplemented diet containing 1.16 % methionine or a normal diet of 0.4 % methionine for 3 months (*ad libitum*) (Niculescu & Zeisel, 2002, Zeisel, 2017). Our data from the 3

months experiment showed that $SR^{-/-}$ mice fed a high methyl donor diet displayed 2.5 fold lower insulin levels compared to $SR^{-/-}$ mice fed a normal diet (**Fig. 7F**). Additional comparisons between WT and $SR^{-/-}$ mice fed a methyl donor diet showed significant differences in insulin levels suggesting that insulin secretion in mice may be under additional regulatory control. We also assayed total DNMT activity in pancreatic nuclear extracts from mice fed high methyl donor and or normal diet to determine rescue of total DNMT activity by providing substrate for the enzymes. $SR^{-/-}$ mice fed a high methyl donor diet showed approximately two fold recovery of total DNMT activity compared to $SR^{-/-}$ mice fed a normal diet (**Fig. 7E**). The difference in DNMT activity was significantly different among WT and $SR^{-/-}$mice in both diet groups (*$p<0.001$). We however did not observe rescue of CREB phosphorylation (S133) in mice fed high methyl donor diet (**Fig. 7G**). These data point to an epigenetic mode of regulation of insulin secretion by SR that involves *Ins1* promoter methylation and DNMT activity.

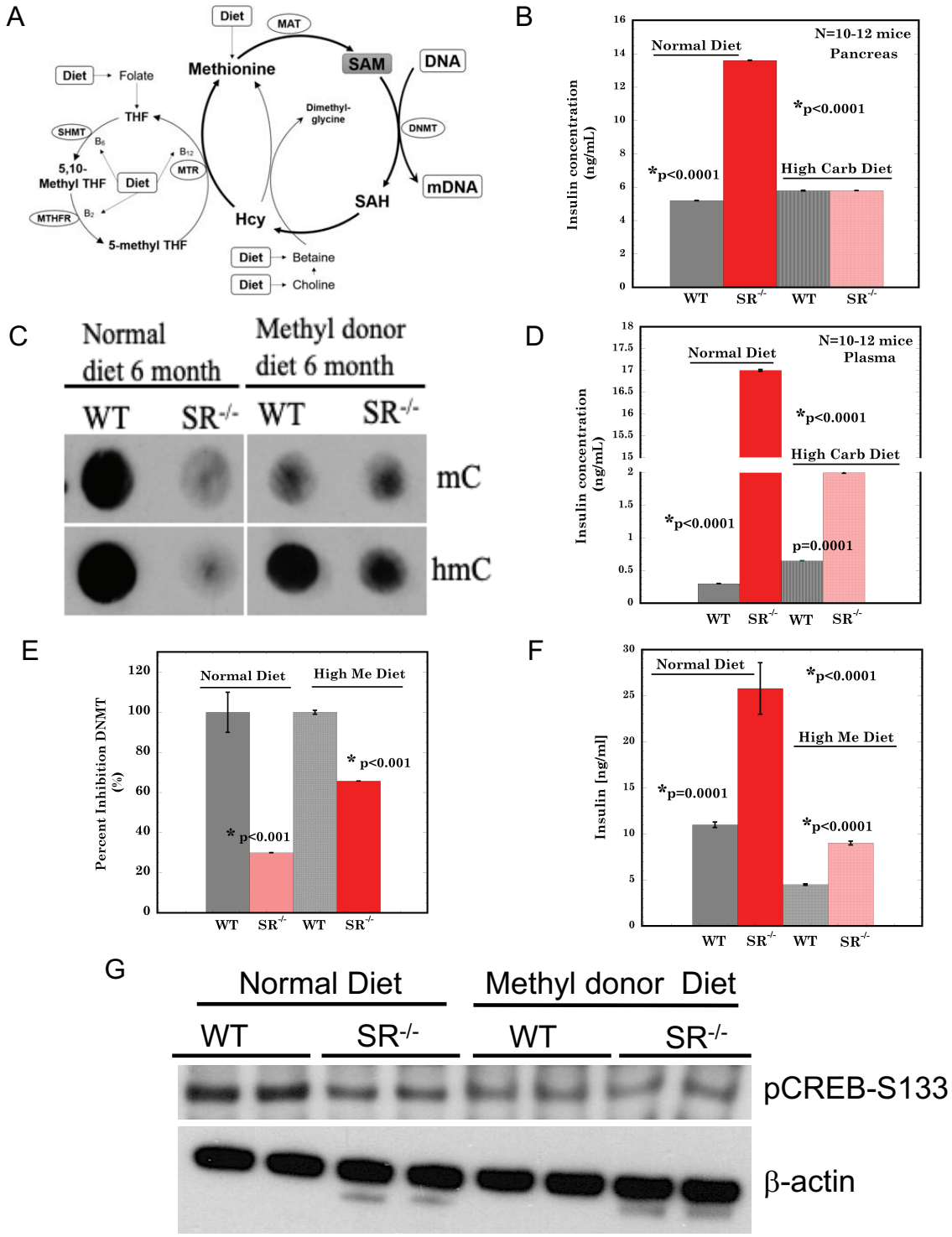

Figure. 7

Figure. 7. Methyl donor dietary supplementation rescues excess insulin production.

Endogenous D-cysteine is transported by ASCT2 and Asc1.

To assess modes of cellular transport of endogenous D-cysteine, we transfected HEK293 cells with ASCT2, a sodium independent transporter that transports D-serine (Kaplan, Zubedat et al., 2018). Our rationale for using HEK293 cells was to use a simple model system to demonstrate transport. The cluster like growth characteristics of β-TC6 cells similar to islets precludes reliable study of transport mechanisms. We incubated cells with 0, 40 and 120 μM concentrations of exogenous D-cysteine for 30 minutes at 37°C. After incubation, we harvested, washed and lysed the cells to measure intracellular D-cysteine using the luciferase assay. ASCT2 transfected HEK293 cells had significantly higher levels of intracellular D-cysteine than untransfected control (**Fig. 8A, 8E**). We performed a similar assay with another class of sodium independent transporter, Asc1. Asc1 transfected HEK293 cells showed significantly higher accumulation of intracellular D-cysteine relative to control (untransfected) (**Fig. 8B, 8E**) (Rutter, Fradley et al., 2007, Sason, Billard et al., 2017). *Ex vivo* experiments in age matched WT and $Asc1^{-/-}$ mice (day 10 old as $Asc1^{-/-}$ mice die by day 14) pancreas showed higher accumulation of intracellular D-cysteine in $Asc1^{-/-}$ mice (1.8 μM) relative to $Asc1^{+/-}$ (0.3 μM) and in WT mice, where the levels of D-cysteine were minimal (**Fig. 8C**) (Xie, Dumas et al., 2005). Western blots of pancreatic lysates of WT and $Asc1^{-/-}$ mice showed that expression of SR was significantly reduced in both the liver and pancreas (**Fig. 8D**). The magnitude of reduction in SR was greater in the pancreas compared to the liver. It has been reported that high levels of D-cysteine (> 1mM) inhibit racemization activity of SR (Dunlop & Neidle, 2005). These data suggest that high levels of intracellular D-cysteine inhibit expression and possibly racemization activity of

SR in the liver and pancreas, which may regulate levels of endogenous D-cysteine *in vivo*.

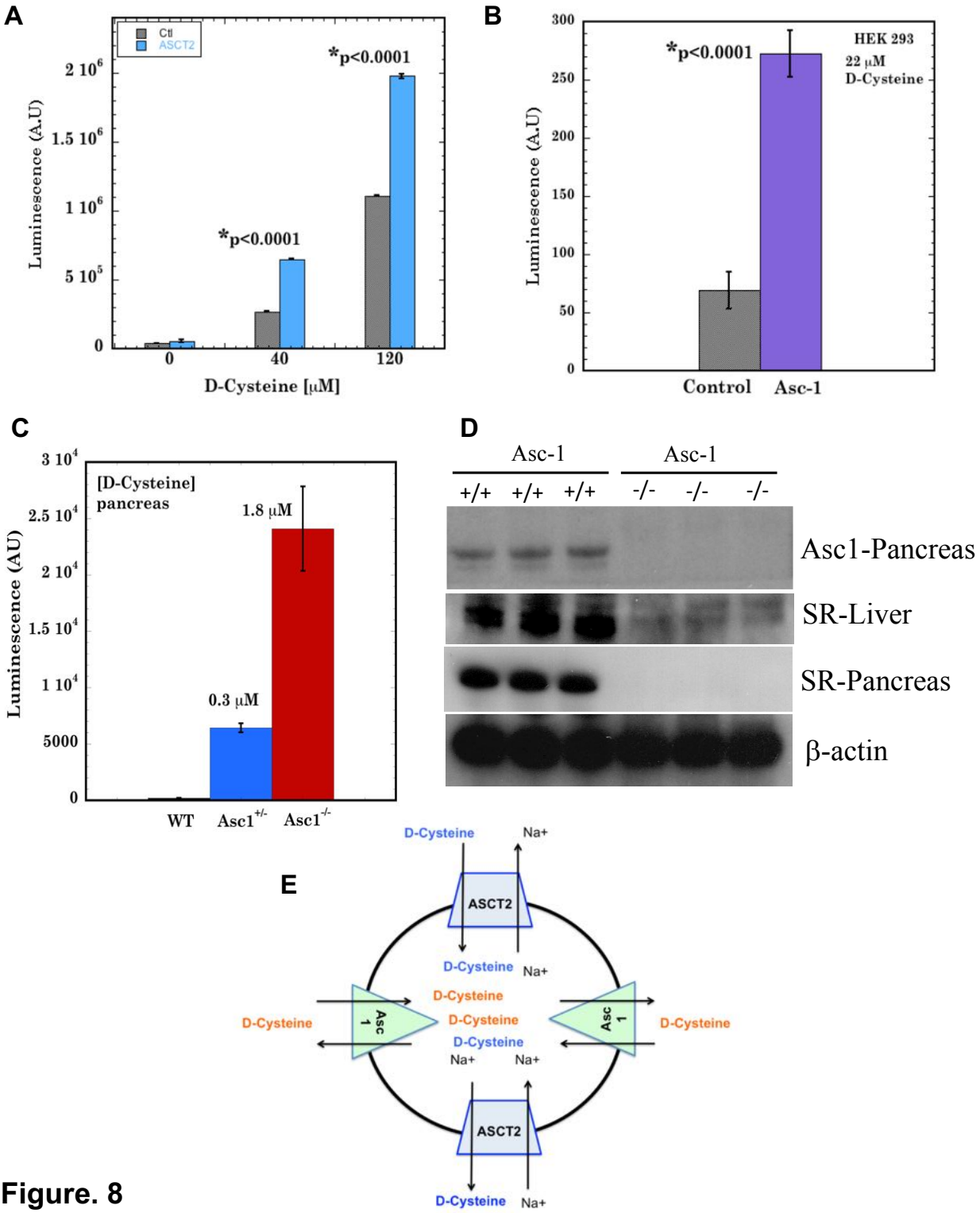

Figure. 8

Figure.8. Endogenous D-cysteine is transported by ASCT2 and Asc1.

In summary our findings show that endogenous mammalian D-cysteine synthesized by SR is enriched in the pancreas where it signals via a cAMP dependent mechanism. Reduced cAMP leads to decreased phosphorylation of CREB at Serine 133, leading to decreased expression of *DNMT*1 and total DNMT enzymatic activity, which is responsible for reduced methylation of the *Ins1* promoter, consequently affecting insulin synthesis and secretion (**Fig. 5E**).

Discussion:

Biological homochirality is a signature of life. The preponderance of L-amino acids in proteins and D-sugars implies most of the biological universe has an inherent disposition towards molecular asymmetry. While L-isomers are present in abundance, their D-counterparts are present in smaller amounts and unlike L-isomers, devoid of higher order assembly in mammals. Prior misconceptions about the existence of D-isomers in only prokaryotes and lower eukaryotes have been dispelled due to the cloning of SR from mouse brain and the identification of D-serine and D-aspartate in the mammalian brain where they function as ligands at the NMDA receptor. In addition, other D-stereoisomers like D-cysteine and D-glutamate have also shown to be present in mammals. Our work identifies the function and basic properties of endogenous D-cysteine synthesized by SR in the pancreas of mice.

Detection of D-stereoisomers by chiral HPLC allows for quantitative estimation in tissues and cells and remains the gold standard. We estimated endogenous D-cysteine using a novel, yet simple bioluminescent luciferase assay, which is stereospecific for D-

cysteine. Our data from the luciferase assay concur with the chiral HPLC data of L and D-cysteine on quantitative estimates of D-cysteine.

In vitro racemization rates show cysteine to be the fastest racemizing among the amino acids with a $t_{1/2}$ of 2 days (Man & Bada, 1987). Since cysteine has a faster *in vitro* racemization rate compared to serine, both of which are structurally similar, its detection may pose a challenge. This may be the reason for the lack of literature on endogenous D-cysteine till now. Due to structural similarities between these two isomers, it is of little surprise that we observed SR to be the biosynthetic enzyme for D-cysteine. Interestingly, even with a difference of a single atom (sulfur versus oxygen), our kinetic data shows that SR has a higher affinity for L-cysteine than L-serine suggesting that it may be a better substrate for SR. Evidence for L-cysteine being a better substrate for SR is also seen indirectly from inhibition studies of L-serine racemization performed in the presence of 10 mM L and D cysteine. In these studies, cysteine was the only amino acid that showed not 50 % inhibition (which would be the case if serine and cysteine were equal affinity substrates for SR), but more than 95 % inhibition of L-serine racemization (Panizzutti et al., 2001). Based on our kinetic data and prior work (Panizzutti et al., 2001), SR also functions as a cysteine racemase. Dual substrate specificity of SR implies that it regulates the concentration of both D-serine and D-cysteine at any given time in the cell. Prior work has suggested that the synthetic profiles of D-cysteine and D-serine are completely opposite during neural development (Semenza et al., 2021).

L-amino acids have been shown to regulate the activity of SR. L-cysteine at a concentration of 1 mM led to a 42 % drop in racemization activity. Interestingly, of all the

molecules studied, the substrates and inhibitors of SR were of L-configuration (Dunlop & Neidle, 2005). D-cysteine was less inhibitory to SR than L-cysteine. In the presence of L-cysteine, there was a decrease in V_{max} of SR without affecting K_m suggesting that the kinetic properties of SR are unaffected. Levels of D-cysteine may also be tightly regulated *in vivo*.

Asc-$1^{-/-}$ mice die by day 14 (Xie et al., 2005). Our transport experiments were performed on ex vivo pancreas from living day 10 Asc-$1^{-/-}$ mice. Endocrine and exocrine pancreatic cell fate determinants are established by E14.5 (Fenech, 2017). Our transport data from Asc$1^{-/-}$ mouse pancreas and HEK293 cells show higher accumulation of intracellular D-cysteine, suggesting that Asc1 is a transporter for D-cysteine. High levels of D-cysteine accumulation also resulted in significant reduction in expression of SR both in the liver and pancreas of Asc-$1^{-/-}$ mice, suggesting feedback inhibition mechanisms that may regulate levels of intracellular D-cysteine. Our studies of D-cysteine transport in HEK293 cells show that both Asc-1 and ASCT2 function as transporters of D-cysteine.Future work may reveal additional classes of transporters of D-cysteine.

D-cysteine is synthesized by SR and the high insulin levels are constitutive as fasting showed no change in plasma insulin levels in $SR^{-/-}$ mice. Constitutively high levels of insulin may pose a health risk. In order to investigate mice tolerance to such constitutively high levels of insulin, we investigated its storage in vivo. Insulin is stored in secretory vesicles of the pancreas and in plasma exosomes in $SR^{-/-}$ mice as amyloid aggregates. Storage of hormones as functional amyloid has been shown to serve as a means of regulating circulating levels in plasma (Maji et al., 2009).

SR epigenetically regulates insulin secretion by decreasing methylation of the *Ins1* promoter in addition to global reduction in methyl and hydroxymethyl cytosine modifications in the pancreatic DNA. The one-carbon metabolism by the folate and methionine cycles integrates inputs from amino acids, glucose and vitamins to generate varied outputs in the synthesis of lipids, nucleotides and proteins, maintenance of redox status and substrate for methylation reactions. Availability of serine is crucial for these two cycles, and in turn determines the synthesis of cysteine via the transsulfuration pathway. Cysteine could also affect serine and methionine synthesis by the reverse transsulfuration pathway. Based on this rationale, we performed an unbiased nucleotide screen using UPLC-MRM MS/MS in the pancreas. Interestingly, we observed significant reductions in a variety of nucleotides including AMP, ADP, GMP, GDP, GTP, dGTP, IMP, dIMP IDP, CTP, TTP and TMP in $SR^{-/-}$ mice. Global decrease in nucleotides is likely to impact the production of a variety of intracellular messengers. We measured the levels of one such second messenger cAMP. cAMP levels were significantly reduced in $SR^{-/-}$ mice suggesting that D-cysteine may signal via cAMP in the pancreas. Live cell imaging monitoring real time dynamics of cAMP showed that stimulation of both HEK293 and βTC-6 cells with D-cysteine resulted in robust enhancement of fluorescence of the cAMP biosensor pink flamindo compared to L-cysteine, implying a stereoselective mechanism of signaling by D-cysteine.

Since there are no reports on endogenous D-cysteine in the pancreas of mammals, we performed a mass spectrometry based global proteomics screen to identify proteins under the control of D-cysteine in the pancreas. Our MS screen found notable upregulation (>2 fold) of islet regenerating factor, cellular transport proteins, ribosomal

proteins, ubiquitination proteins and chaperones in $SR^{-/-}$pancreas. Interestingly, among the proteins that were downregulated was cytosolic 10-formyl tetrahydrofolate dehydrogenase (fivefold downregulation), which, is involved in mitochondrial 1C metabolism and controls SAM levels. Based on this rationale, we investigated DNA methylation in the pancreas and found a decrease in global levels of mC and hmC modifications in the DNA of $SR^{-/-}$ pancreas by DNA dot blot in addition to lower levels of methylation of the *Ins1* promoter by bisulfite sequencing. Our data suggest that hypomethylation of the *Ins1* promoter in $SR^{-/-}$ mice could be a plausible explanation for the higher insulin levels in $SR^{-/-}$ mice.

In order to further elaborate our mechanism, we determined levels of total CREB and phospho CREB (S133) and found lower levels of both in $SR^{-/-}$ both in total pancreatic and nuclear extracts. CREB is a transcription factor that controls *DNMT1* expression (Impey et al., 2004). Expression of DNMT1, 3A and 3B enzymes were decreased in $SR^{-/-}$ pancreas, resulting in reduced total DNMT activity. Our data suggests that lower levels of CREB and phospho-CREB (S133) may affect the incorporation of methyl groups in the $SR^{-/-}$ DNA due to lower activity and expression of DNMT1 and the 5 fold downregulation of cytosolic 10-formyl tetrahydrofolate dehydrogenase involved in folate metabolism.

A strong test for a hypothesis is ensuring a complete or partial restoration of optimal biological function when provided with the missing component. To test our DNA methylation hypothesis in controlling insulin secretion, we performed two rescue experiments by providing methionine as a source of methyl donors. Our rationale was that dietary supplementation of methionine may provide the necessary substrate for the

generation of SAM and therefore lead to optimal methylation of DNA by DNMT enzymes and control insulin levels. However, a challenge with such dietary supplementation studies is the dose and duration of these experiments to observe efficacy. Methionine is among the most toxic amino acid in mammals (Ishii, Kamata et al., 2022). We selected the concentration of methionine in our rescue experiments based on current mice dietary guideline formulation for tolerance in mice. Our 6 month high carbohydrate and high methyl donor dietary supplementation experimentation led to a significant decrease in insulin levels both in the pancreas and plasma of $SR^{-/-}$ mice. The shorter 3 month supplementation exclusively with high methyl donors (1.18% methionine versus 0.8 % in the high carb diet) showed approximately 3 fold reduction in pancreatic insulin levels in mice fed a high methyl diet and was equally effective as the longer duration experiment. The rationale for the shorter experiment was to ensure that the rescue effects observed was due to methionine and not high carbohydrate. Interestingly, WT control mice fed a high methyl donor diet also showed reduction in insulin levels suggesting that its synthesis and secretion is also regulated epigenetically, in addition to other modes of regulation. There was also a partial rescue of total DNMT activity (more than 2 fold compared to control) in mice fed a high methyl donor diet. Rescue of phosphorylation of CREB S133 was however not seen in the 3 months rescue experiment. Global mC and hmC levels in the 6 months experiment also showed partial rescue of modification in the DNA of mice fed a high methyl donor diet. Collectively, our rescue experiments clearly demonstrate that SR controls methylation specifically of the *Ins1* and other promoters in the pancreas.

DAO regulates the concentrations of various D-amino acids *in vivo*. Our kinetic data comparing the activity of purified DAO showed that it is equally efficient at degrading D-cysteine and D-serine. A prior study showed that competition assays between D-serine and D-cysteine had no effect on the activity of DAO suggesting that D-cysteine may be a better substrate then D-serine (Bailey et al., 2015).

Nothing is known about endogenous D-cysteine in the mammalian pancreas. Our MS based proteomics screen show that D-cysteine may play roles in cellular metabolism, actin cytoskeleton assembly, folate biosynthesis and mitochondrial electron transfer, implying novel functions. Characterizing the functions of D-cysteine may elucidate its novel roles in the pancreas. Cysteine has additional metabolites like cysteic acid, cystine and homocysteine. The D stereoisomers of these metabolites could potentially regulate insulin levels in mammals with roles in islet development.

In conclusion endogenous mammalian D-cysteine is synthesized by SR which physiologically downregulates insulin promoter methylation and signals via cAMP, CREB and DNMT1 interaction. We focus on D-cysteine, due to higher affinity of L-cysteine as a substrate for SR. Prior work has shown that absence of D-cysteine leads to hyperproliferation of mouse neural progenitor cells in the brain leading to aberrant cortical layering (Roychaudhuri & Snyder, 2022, Semenza et al., 2021). D-cysteine may play analogus roles in the pancreas during development, controlling islet cell proliferation and possibly insulin secretion. Regulating the activity of SR and D-cysteine synthesis by inhibitors may have therapeutic implications for glucose homeostasis and possibly type 1 diabetes.

Materials and Methods

Reagents and Antibodies: Purified L-cysteine, D-cysteine, L-serine, D-serine, CHBT (cyano hydroxy benzothiazole) were purchased from Sigma Chemical Corp. TCEP HCl (Tris (2-carboxy ethyl phosphine) hydrochloride) was purchased from Thermo Scientific. All salts for buffers and reagents were of research grade and high purity. Milli Q water was used to make buffers and solutions for experiments. HPLC grade solvents and water (Fisher Scientific) was used for HPLC estimation of D and L-Cysteine. Anti-conjugated D-cysteine antibody (AB-T050; Advanced Targeting Systems, San Diego, CA). Anti cAMP mouse monoclonal antibody (MAB2146-SP; Novus Biologicals). Rabbit anti DNMT1antibody (Aviva; ARP37033_P050), mouse anti DNMT3A (PCRP-DSHB Iowa), rabbit anti DNMT3B antibody (GeneTex; GTX 129127), rabbit anti CREB (CST; 48H2), rabbit anti phospho-CREB (S133) (CST; 87G3), rabbit anti SR antibody (CST; D5V9Z), rabbit anti SLC7A10 polyclonal antibody (G-Biosciences; ITA8971).

Extraction of D-cysteine: D-cysteine was extracted from age matched WT and $SR^{-/-}$ mice and rabbit pancreas after dissecting out the organ followed by homogenization in 5 volumes (w/v) of reaction buffer containing 500 mM tricine, 100 mM magnesium sulfate, 2 mM EDTA, 1% Triton X-100. Stock solutions of 100 mM TCEP, 1 mg/ml CHBT and 2 M Na_2CO_3 were added to the reaction buffer at $1/10^{th}$ volume of the homogenization buffer. Tissues were homogenized using a handheld homogenizer and on ice till the sample formed a uniform suspension. The homogenates were sonicated using a sonicator probe on ice for 6 pulses with each pulse lasting 10 seconds. The sonicated samples were incubated at 30°C thermomixer at 1100 rpm for 10 minutes. The samples

were centrifuged at 16,000 g for 30 minutes at 4°C and supernates harvested carefully and stored on ice prior to performing the luciferase assay.

Luciferase Assay: Luciferase assay was performed on the supernates after extraction by adding a fixed volume of supernate and neutralizing it with 10N HCl (for 1000 µl supernate: 15 µl HCl). The pH was determined using a Whatman pH paper (pH 7.0-8.0). After neutralization, depending on the volume of supernate, 1/10th (v/v) 50 mM Mg-ATP was added followed by 1 mg/ml stock solution of firefly luciferase (1/1000 v). The sample was gently mixed and 200 µl transferred to each well of a 96 well opaque plate and luminescence measured. The luminescence was corrected using a buffer blank treated identically and the data plotted. Quantitative estimation of D-cysteine was based on a standard curve generated using lysates from the respective organ (Bailey et al., 2015, Corrigan, 1969, Niwa et al., 2006).

Insulin ELISA: Quantitative estimation of insulin from plasma and pancreas was performed using the Ultra Sensitive Mouse Insulin ELISA Kit (Cat# 90080; Crystal Chem). The protocol was followed exactly as mentioned for the high range assay. Standard curve for insulin was developed prior to the actual experiment (high range). Each individual sample was done in quadruplicate. For treatment groups, the samples were pooled in their respective groups and analyzed. The absorbance was read at 450 nm in a 96 well plate reader and also at 630 nm and data plotted after correction at 630 nm.

Analysis of Gene expression: RNA was isolated from pancreas, islets and acinar cells from WT and $SR^{-/-}$ mice using RNeasy Mini kit (Qiagen). Gene expression studies related to glucose homeostasis and pancreas development were performed using the SYBR green method. cDNA synthesis was performed using High Capacity cDNA synthesis kit (Applied Biosystems). 100 ng of synthesized cDNA was used in each well of a 96 well 0.1 ml MicroAmp PCR plate (Applied Biosystems) along with SYBR Green master mix, nuclease free water and gene specific primers (10 □M final concentration). 18S rRNA was used as a housekeeping gene and non-template control was added in each plate as a control. The PCR was run on an ABI Step One Plus instrument. The raw data obtained was analyzed on StepOne data analysis software (StepOne Plus) and mean C_T values obtained. ΔC_T and $\Delta\Delta C_T$ were calculated and fold change in gene expression obtained from $2^{exp-\Delta\Delta CT}$.

Glucose Tolerance Tests: Glucose tolerance test (GTT) was performed on a 16 h fasted WT and $SR^{-/-}$ age matched mice injected i.p with D-glucose (2 g/kg body weight). Blood glucose level was monitored by tail bleeding immediately before and at indicated times after injection using Contour glucometer (Bayer Co, Japan) and Contour blood glucose test strips (Cat#7097C; Ascensia Diabetes care Inc, NJ). Blood glucose measurements were obtained from tail veins at indicated time points post injection. A small drop of blood from the tail was placed on a new glucose strip each time, inserted into the glucometer and value recorded.

Plasma fasting Insulin: Age matched WT and $SR^{-/-}$ mice (8-12 weeks old) were fasted for 16 h with only access to water. Mice were euthanized and blood obtained by cardiac puncture using a 1 ml tuberculin syringe (BD Biosciences). The harvested blood was stored in a BD Microtainer tube (cat# 365985) with lithium heparin on ice. Plasma was obtained by centrifuging the microtainer tubes at 3000 rpm for 15 minutes at 4°C. After centrifugation the cell free supernatant layer (plasma) from the top was carefully removed into a tube containing protease inhibitors (1:20 v/v) and kept on ice. The isolated plasma was assayed for insulin using mouse insulin ELISA as mentioned. Plasma insulin levels during the GTT were assayed in an exactly similar fashion after administering the required dose of glucose. Plasma for each genotype was pooled from N=5-8 mice and assayed in triplicate or quadruplicate in a 96 well format. Data were subtracted from blank wells containing sample diluent alone. Error bars obtained refer to SD. The experiment was independently performed 3 times.

Glycogen Estimation: Glycogen was estimated from age matched WT and $SR^{-/-}$ mouse liver. A small portion of the liver (approx. 0.5-1 g wet tissue) was dissected and minced in a petri dish and dissolved in 4 times the volume (w/v) of 10 % perchloric acid and homogenized in a handheld homogenizer. Following homogenization, the sample was centrifuged at 300 g for 10 minutes. A portion of the supernate was extracted with 1:1 (v/v) ethanol and centrifuged at 1700 g for 10 minutes at 4°C. The supernate was discarded and the pellet resuspended in the same volume of water as the initial volume of supernate (approx. 200 μl). Fifteen μl of the supernate was removed for assay in a 96 well plate. The sample was diluted in 15 μl water followed by addition of 30 μl 6.5 %

phenol and 150 µl of 85 % sulfuric acid in a total volume of 210 µl. The samples were run with an N=5 replicates. Blank wells contained water instead of sample. The plate was read in a 96 well plate reader at 420 nm and the amount of glycogen quantified based on a standard curve (Rasouli et al., 2014).

Estimation of ketone bodies by NMR: Ketone bodies extraction and estimation from livers of WT and $SR^{-/-}$ mice was performed using ^{1}H NMR at the Metabolomics Innovation Centre (TMIC, Canada). Briefly, samples were extracted and prepared as mentioned in [26]. The tissue was homogenized and fractionated to obtain a biphasic mixture. The upper polar phase (water-soluble metabolites) and lower non-polar phase (lipid-soluble metabolites) were carefully separated. The water-soluble tissue extract was transferred to a 1.5 ml eppendorf tube, to which an additional standard NMR buffer solution was added. The buffer consisted of 750.0 mM potassium phosphate (pH 7.0), 5.0 mM 2,2-dimethyl-2-silapentane-5 sulfonate (DSS-d6), 5.84 mM 2-chloropyrimidine-5-carboxylic acid, and D_2O (54 % v/v in H_2O). All ^{1}H-NMR spectra were collected on a Bruker Avance III Ascend 700 MHz spectrometer equipped with a 5 mm cryo-probe (Bruker Biospin, Rheinstetten, Germany). ^{1}H-NMR spectra were collected at 25 °C using the first transient of a noesy-pre saturation pulse sequence. This pulse sequence was selected based on its excellent reproducibility and quantitative accuracy. NMR spectra were acquired with 128 scans employing a 4 second acquisition time and a 1 second recycle delay. Prior to spectral deconvolution, all free induction decays (FIDs) were zero-filled to 240,000 data points and a 0.5 Hz line broadening function was applied. The methyl singlet of the added DSS (set to 0.00 ppm) served both as an

internal chemical shift referencing standard and as an internal standard for quantification. All ^{1}H-NMR spectra were processed using the Chenomx NMR Suite 8.1 software package (Chenomx Inc., Edmonton, Canada) for compound identification and quantification as described [26].

Quantitative proteomic analysis by nano LC-MS/MS: Global proteomic analysis of pancreatic lysates from WT and $SR^{-/-}$ mice was performed on a nano LC-MS/MS platform by Creative Proteomics (45-1 Ramsey Road, Shirley, NY 11967, USA). The tissues were lysed in lysis buffer containing 8M urea with 1% protease inhibitor and 1% phosphatase inhibitor by sonication. Samples were centrifuged at 12,000 g for 10 minutes at 4°C and supernates harvested. Protein concentration was estimated using BCA kit. Protein digestion was performed after reduction (by 10 mM DTT) and alkylation (by 20 mM iodoacetamide) by trypsin at 37°C with overnight incubation at a trypsin: sample ratio of 1:50. Samples were centrifuged at 12,000 g at 4°C for 10 minutes. The sample was lyophilized and resuspended in 20 μl of 0.1% formic acid before LC-MS/MS. LC-MS/MS was performed on Ultimate 3000 nano UHPLC system (ThermoFisher Scientific, USA) with an analytical PepMap C_{18} column. Mobile phase A was 0.1% formic acid in water and B was 0.1% formic acid in 80 % acetonitrile. Flow rate was 250 nL/min. MS was performed on an Orbitrap Q HF mass spectrometer (ThermoFisher Scientific, USA) with a spray voltage of 2.2 kV and capillary temperature of 270°C. MS resolution was 60000 at 400 m/z and MS precursor m/z range was 300.0-1650.0. For data dependent MS/MS, up to top 20 most intense peptide ions from the preview scan in Orbitrap was selected. Data analysis following LC/MS-MS was

performed using Maxquant (1.6.2.6) against a mouse protein database. The protein modifications were carbamidomethylation (C) (fixed), oxidation (M) (variable); enzyme specificity was set to trypsin; maximum missed cleavages were set to 2; the precursor ion mass tolerance was set to 10 ppm, and MS/MS tolerance was 0.6 Da. Only highly confident identified peptides were chosen for downstream protein identification analysis (Bian et al., 2020).

DAO (D-amino acid oxidase) assay: Equimolar amounts of D-cysteine and D-serine (20-500 μM) was prepared in water and diluted in 100 mM Tris buffer pH 7.5 and added to 0.026 μM (0.2 μg protein in 200 μl total reaction volume) purified porcine DAO in 100 mM Tris buffer pH 7.5, 100 μM FAD, 100 μM NADPH followed by 1 μg glutamate dehydrogenase (Sasamura et al., 2002). The assay for each substrate was performed separately in a 96 well black clear bottom plate. The plate was incubated at 37°C for the duration of the assay and read at t=0, 2, 4, 6, 8, 10, 15, 20, 25, 30, 40, 50 and 60 minutes at 340 nm. The decrease in absorbance was followed and data plotted to obtain the kinetic parameters.

Purification of mouse Serine Racemase (SR): Mouse SR (pcDNA3.1 His tag expression vector) was expressed and induced in BL21 (DE3) competent *E. coli*. A colony was inoculated into 100 ml of LB medium with 50 ug/ml of kanamycin for 18 hrs. Later, the cells were expanded to an 8 L culture. When the OD reached 0.4, 0.2 mM ITPG was added and the cells were grown at 18°C, 200 rpm for 18 h. Cells were centrifuged at 10,000g and the pellet was frozen at -80°C. Cells were lysed with a

microfluidizer and lysis buffer (50 mM Tris pH 8.0 containing 150 mM NaCl + 1 mM TCEP and 15 μM PLP). The supernatant was passed through a 5 ml Ni^{2+} affinity column (GE Healthcare) and eluted with the same lysis buffer containing imidazole. The protein eluted at about 200-250 mM imidazole. The relevant fractions were identified by SDS-PAGE, pooled and concentrated to 10 ml and applied to a 320 ml size exclusion column (HiLoad ® 26/600 Superdex ® 200, GE Healthcare). The column was equilibrated with 30 mM PIPES pH 7.4 buffer containing 100 mM NaCl + 1 mM TCEP+ 15 μM PLP and eluted with the same buffer. Fractions of 8 ml were collected in an automated AKTA FPLC system (GE Healthcare) and purity was determined with SDS-PAGE. Purified mouse SR was concentrated using a Pierce protein concentrator (Thermo Scientific) 10K molecular weight cut off filter. The concentration was determined using a UV spectrometer and an extinction coefficient of 31775 M-1 cm-1. The concentrate was assayed for amount of protein and used in enzyme kinetic assays.

Serine racemase luciferase assay: Racemization of L-cysteine to D-cysteine was measured using the luciferase assay for D-cysteine (Bailey et al., 2015, Corrigan, 1969, Niwa et al., 2006). Purified serine racemase (2 μg protein) was incubated at 37°C with 50 μM PLP, 1 mM Mg^{2+} and 100 mM Tris-Cl pH 7.8 buffer along with 200 μM L-cysteine as substrate in a total volume of 600 μl. Concentration of reagents mentioned are final concentration in the assay. At 5, 10, 15, 30 and 60 minutes, an aliquot of the reaction mixture (100 μl) was removed and subjected to the luciferase assay (as mentioned above) to measure the amount of D-cysteine produced using bioluminescence. The amount of D-cysteine estimated using a standard curve was plotted versus time.

Serine racemase amplex red assay: Racemization of L-cysteine or L-serine to D-cysteine or D-serine was measured using amplex red assay (Nelson et al., 2017, Tomoko Naka, 2010). Purified serine racemase (5 μg protein/well) was pre incubated for 20 minutes at 37°C with 15 μM PLP, 1 μM Mg^{2+}, 3 mM DTT and 100 mM Tris-Cl pH 8.9 buffer. Following incubation, 50 μM amplex red was added, followed by 2 μg horseradish peroxidase, 100 μM FAD and 1 μg D-amino acid oxidase followed by different concentrations of L-cysteine and or L-serine substrate (0-400 μM) was added in a black 96 well plate. Reagents are final concentration in 200 μl total volume in each well. At specified time intervals (0, 15, 30, 60 and 90 minutes), the plate was read in a microplate reader under fluorescence settings at ex λ 530 nm and em λ 590 nm. Blank wells contained all reagents except enzyme, pyridoxal phosphate (PLP) and flavin adenine dinucleotide (FAD). Blank fluorescence was subtracted from the reaction wells at each time point. Assay was performed in triplicate for each substrate concentration.

Immunohistochemistry: Immunohistochemical experiments were performed on WT and $SR^{-/-}$ mice pancreas. Briefly, the mice were euthanized by CO_2 narcosis and the pancreas removed under a dissecting microscope and incubated in 4 % paraformaldehyde in PBS at 4°C for 48 h with gentle shaking. The tissue was paraffin embedded and sectioned at the Johns Hopkins Oncology Core Services. The sections were de paraffinized using Histoclear followed by a series of 5 min washes in absolute alcohol, 95% alcohol and PBS. Permeabilization of sections was done in 0.5% Triton X-100 in PBS for 20 min. Antigen retrieval was done in 10 mM sodium citrate buffer

containing 0.05 % Tween 20 pH 6.0 by boiling sections for 1 min in the microwave and then cooling at room temperature (RT) for 20 min. Primary antibody dilutions were at 1:500 in 1% BSA in PBS while secondary antibody dilutions were done at 1:1000 in the same buffer. The sections were washed twice in PBS after incubation with primary and secondary antibodies. Hoechst dye was used for nuclear staining. The slides were observed by confocal microscopy.

Global DNA mC and hmC analysis: To determine global methylation (mC) and hydroxymethylation (hmC) of cytosine in DNA, dot blot was performed on DNA isolated from pancreas of age matched WT and $SR^{-/-}$ mice. DNA was isolated using Pure Link Genomic DNA isolation kit (Invitrogen; ThermoFisher Scientific) and quantified using a nanodrop. Nitrocellulose (NC) membrane was wet in 20X SSC buffer at RT for 10 minutes along with a same size Whatman filter paper. The prewet NC membrane along with the filter paper was placed in a spot blot (Schleicher & Schuell, Keene, NH) micro sample filtration manifold. Five hundred μl of 20X SSC buffer was added to each well in which the sample would be added and allowed to drain under suction. DNA samples (200 ng) were prepared for application to the slot by adding 20X SSC buffer to give a final concentration of 6X SSC in a total volume of 200 μl. The DNA was denatured by heating it at 100°C for 10 min and placed on ice. An equal volume of 20X SSC buffer was added to the sample and mixed. The DNA sample was centrifuged for 5 sec and then applied to the prewet wells and allowed to drain completely till the membrane was dry. The NC membrane was removed from the manifold and incubated in a petri dish containing filter paper soaked in denaturation solution (1.5M NaCl + 0.5 M NaOH) for 10

min. The membrane was next transferred to a similar petri dish containing neutralization solution (1.0 M NaCl + 0.5 M Tris-Cl pH 7.0) and incubated for 5 min. After incubation, the membrane was placed on a filter paper prewet with 20X SSC buffer with DNA side up and crosslinked using a Stratalinker UV Crosslinker in the auto crosslink mode (preset exposure of 1200 microjoules x100). The crosslinking time was 25-50 seconds. The crosslinked DNA on the NC membrane was placed in blocking buffer (5% BSA (w/v) in TBS-T) and incubated at RT for 30 min on a shaker. Primary antibodies to mC (Cat# A-1014; Epigentek Inc) and hmC (Cat# A-1018; Epigentek Inc) were added separately to the membranes at 1:2000 dilution in blocking buffer and incubated at 4°C overnight with gentle shaking. The membranes were washed 4 times 15 min each at RT with shaking in TBS-T following which they were incubated with respective secondary antibodies at 1:5000 dilution in blocking buffer for 60 min at RT. The membranes were washed 4 times as mentioned above and developed using ECL reagent (Super Signal West Pico Plus) for 5 min and membranes developed in the dark using X-ray film.

Targeted Bisulfite sequencing of Insulin promoter: Gene-specific DNA methylation was performed by CD Genomics Co (Shirley, NY) on DNA samples from pancreas of age matched WT and $SR^{-/-}$ mice. DNA methylation was assessed by a next generation sequencing based bisulfite sequencing based PCR (BSP) according to previously published methods (Gao et al., 2015, Lister et al., 2009, Olova et al., 2018). BSP primers were designed using the online MethPrimer software. Genomic DNA (1 μg) was converted using the ZYMO EZ DNA Methylation-Gold kit (ZYMO) and one twentieth of the elution products were used as templates for PCR amplification. For each sample,

BSP products of multiple genes were generated, pooled equally and subjected to adapter ligation. Barcoded libraries from all samples were sequenced on the Illumina Hiseq platform using paired-end 1150 bp strategy. After the preparation of the library, Qubit 2.0 and Agilent 2100 were used respectively to detect concentration of the library and insert size. Effective concentration (> 2 nM) of the library was quantitatively determined by qPCR to ensure library quality. The original data obtained from the high throughput sequencing platforms were transformed to sequenced reads by base calling. The level of methylation at each site of the insulin promoter between sample groups were statistically analyzed based on the methylation level of each site and data plotted with *p* values for N=2 samples per genotype.

Dietary supplementation studies: 8 weeks old age matched WT and $SR^{-/-}$ mice were fed 70% carbohydrate diet containing 0.8 % methionine (Teklad Custom Diet TD.98090, Envigo, WI) for 6 months. Sufficient quantities for food was maintained in the cages and the food replaced every week for the entire duration of the experiment. Control mice were fed normal chow (Teklad Global 18% Protein Rodent Diet, 2018S, Envigo, WI) containing 0.6 % methionine. The normal diet was replaced at regular intervals by the animal care staff as per IACUC regulations. After completion of 6 months, blood glucose was measured and subsequently the animals euthanized by CO_2 narcosis. Plasma was isolated by cardiac puncture and harvested using a butterfly needle attached to a 1ml syringe. The blood was collected in a lithium heparinized tube (BD Microtainer; REF 365965) and placed on ice. The tubes were centrifuged at 3000 rpm for 15 minutes at 4°C and the supernatant isolated in a separate tube containing proteinase inhibitors

(Sigma Protease Inhibitor Cocktail). In addition to plasma, the pancreas was removed for ELISA and mC (methyl cytosine) and hmC (hydroxymethyl cytosine) based DNA dot blot analysis. All groups had a minimum of 12-15 mice per group.

In a separate shorter duration experiment (3 months), 8 weeks old age matched WT and $SR^{-/-}$ mice were fed a 3X methyl supplemented (3MS) diet containing 17.3 g choline, 15 g betaine, 7.5 g methionine (1.15 % methionine), 0.015 g folic acid, 1.5 % Vit B_{12} and 0.661 g zinc sulfate heptahydrate (Teklad Custom Diet T.110835, Envigo, WI) for 3 months along with age matched control mice that were fed normal chow for the same length of time (Niculescu & Zeisel, 2002). After completion of 3 months, similar parameters as above were measured to determine extent of rescue. All study groups had a minimum of 12-15 mice.

Separation of L and D cysteine: Purified L and D cysteine were separated using the Astec Chirobiotic T chiral HPLC column (5 μm particle size, L x 1.D. 25 cm x 4.6 mm) (Suppelco) attached to a Waters 2690 alliance separations module connected to a fluorescence detector with 80-20 % (v/v) 20 mM ammonium acetate-methanol solvent by isocratic elution. The flow rate of the solvent was 0.1 ml/min. The eluates were detected by fluorescence with excitation λ 380 nm and emission λ 510 nm. The column was maintained at room temperature. Both L and D Cysteine from liver and pancreatic homogenates were extracted by homogenization in 100 mM HEPES buffer pH 7.5 using a handheld tissue homogenizer on ice with 10-15 strokes. The homogenates were then lysed using a sonicator three times with a pulse of 10-15 sec per pulse on ice. The samples were then centrifuged at 16,000 g for 30 min at 4°C. After centrifugation the

supernate was harvested in a pre-chilled tube. Proteins in the supernates were precipitated by adding 12 N HCl to the lysate to give a final concentration of 2 N HCl. The sample was cooled on ice for 30 min and centrifuged at 16,000 g for 30 min at 4°C. The supernate was harvested that contained the stereoisomers of cysteine. The supernatant was neutralized by adding one equivalent NaOH (v/v) of 10 N NaOH followed by addition of 1 volume equivalent (v/v) of 1 mM ABDF (4-(aminosulfonyl)-7-fluoro-2,1,3-benzoxadiazole) in 200 mM sodium borate buffer pH 8.0 containing 1 mM EDTA and 0.1 volume equivalent (v/v) of 10 % tri-n-butyl phosphine in acetonitrile (*10*). The mixture was incubated in a 50°C water bath for 5 minutes and vortexed thoroughly after incubation. The mixture was placed on ice and 0.01 volume equivalent (v/v) of 2.5 N HCl added. The fluorescently labeled sample was used for injection on the chiral HPLC column and the ABD adducts detected using fluorescence. The areas under the respective peaks were quantified based on a standard curve of purified L and D cysteine.

Western blot: Pancreatic and islet lysates were run on a 1 mm 4-12% Bis-Tris gel (Novex Life Technologies; Thermo Fisher; #NP0321) with MES SDS running buffer (Invitrogen; #NP0002-02) initially at 75 V and then at 120 V. The samples were then transferred to a prewet immobilon PVDF transfer membrane (Merck Millipore Ltd; #IPFL00010; Pore Size 0.45 μm) and sandwiched between wet filter paper and cassette holder. The entire apparatus was placed in a wet transfer apparatus (Bio-Rad) and run at 90 V for 90 min on ice. After transfer, the membrane was removed and incubated in blocking buffer containing Tris buffered saline + Tween 20 (TBS-T) containing 5% BSA

for 30 minutes at room temperature (RT). The membrane was incubated on a shaker with the respective primary antibody at 1:1000 dilution in blocking buffer overnight at 4°C. After overnight incubation, the membrane was rinsed 3 times with TBS-T and washed in TBS-T at RT for 15 minutes per wash. The membrane was washed a total of 4 times. After washing, the membrane was incubated with HRP conjugated secondary antibody (IgG; mouse or rabbit) (GE Healthcare UK) at 1:5000 dilution in blocking buffer and incubated at RT with shaking for 1 h. After incubation with secondary antibody, the membrane was washed 4 times with TBS-T. The duration of each wash was 15 min. After the last wash, the membrane was incubated with Enhanced Chemiluminescent (ECL) reagent (Thermo Scientific; Super Signal West Pico Plus Peroxide solution (#1863099) and Luminol enhancer solution (#1863098) in a 1:1 (v/v) for 5 min in the dark. The excess ECL reagent was removed using a kimwipe and the membrane was placed in between plastic sheet in a cassette holder and developed on an 8" X 10" UltraCruz autoradiography film (Santa Cruz Biotechnology; #SC-201697) in a developer.

Dot Blot of Secretory Vesicles and Exosomes: Dot blotting of secretory vesicles and plasma exosomes was performed on a prewet PVDF membrane treated with methanol, water and transfer buffer. The wet PVDF membrane was then place in a 96 well microsample filtration manifold (Schneider & Schuell, NH) attached to a vacuum line. The samples were then added to each well under suction. The suction was done till the samples were adsorbed on the membrane and the membrane dry. The microfiltration apparatus was then disconnected from the vacuum line and the PVDF membrane

gently removed. The membrane with sample spots was then incubated in blocking buffer (5 % BSA+TBST) at room temperature with shaking for 30 minutes. Primary antibodies (rabbit insulin antibody: #4590 Cell Signaling Technology, OC (generic amyloid antibody) and rabbit β-actin antibody; #AC026 AB clonal) were added to the membrane at 1:1000 dilution and incubated overnight with shaking at 4°C. After incubation, the membrane was washed 4 times with TBST at RT for 15 minutes each. The membrane was then incubated with respective secondary antibodies at 1:5000 dilution in TBST at RT for 60 minutes. The blot was then washed 4 times with TBST at RT for 15 minutes each and developed using chemiluminescence with Enhanced Chemiluminescent (ECL) reagent (Thermo Scientific; Super Signal West Pico Plus Peroxide solution (#1863099) and Luminol enhancer solution (#1863098) in a 1:1 (v/v) for 5 min in the dark. The blot was exposed to X-ray film in the dark and developed.

Isolation of Secretory Vesicles from βTC-6 cells: βTC-6 cells were grown in 30 cm dishes at 37°C, 5 % CO_2, for 5-7 days in Dulbecco's Modified Eagle's essential medium (GIBCO, Grand Island, NY) supplemented with 15 % fetal bovine serum. Isolation of and purification of secretory granules from these cells were performed according to Hutton *et. al* (Hutton et al., 2009) with slight modifications. Briefly, the cells were harvested and rinsed with PBS. After washing with PBS, the cells were resuspended with 1X hypotonic medium (2X medium: 60 % sucrose+ 100 mM EGTA-K+-1M $MgSO_4$+ 100 mM MES in 50 ml water). The cells were homogenized in hypotonic medium using a Dounce homogenizer (Wheaton; Milville, NJ) with 20 strokes and on ice. The homogenate was centrifuged at 800 g for 5 min at 4C°. The supernatant was retained.

The pellet was resuspended in original volume of hypotonic medium and centrifuged at 800 g for 5 min. The supernate was pooled from the first spin and centrifuged in a 13 x 56 mm polycarbonate centrifuge tube at 20,000 g at 4°C for 10 min in a Beckman SW55.TI rotor. The supernate was discarded and the pellet resuspended thoroughly in hypotonic medium. The pellet (500 μl volume) was then added to a new polycarbonate tube and underlayed with 3 ml isotonic 30 % Percoll mixed and centrifuged for 60 min at 25,000 g, 4°C in a SW55.TI rotor. After the spin, the gradient was fractionated and 200 μl aliquots sequentially discarded from the top till the last 800 μl was reached. The secretory vesicles were present in this fraction at the bottom of the tube. The secretory vesicle fraction was then centrifuged in the same tube for 10 min at 20,000 g and pellet stored at -80°C or used immediately for experiments.

Isolation of plasma exosomes. Exosomes from mice plasma were harvested from age matched WT and $SR^{-/-}$ mice (6-8 weeks) plasma using the total exosome precipitation reagent for plasma (Invitrogen #4484451) as per instructions. Plasma was isolated on the same day of exosome isolation or kept at -80°C and thawed on the day of isolation of exosomes.

Thioflavin T binding: Plasma exosomes and secretory vesicles from βTC-6 cells were assayed for β-sheet aggregates using ThT binding (Biancalana & Koide, 2010, Roychaudhuri et al., 2014). All samples were assayed in quadruplicate with 10 μg of protein per well of a 96 well optical bottom microtiter plate (Thermo Fisher Scientific, Rochester NY). The total volume per well was 200 μl comprising 10 μg of exosome

lysate or βTC-6 secretory vesicle lysate followed by ThT dye (final concentration of 1 mM) and PBS. The samples were mixed by pipetting and read immediately and subsequently at regular intervals at λex= 450 nm and λem=482 nm. During the readings the plate was incubated at 37°C without shaking. The mean of the blank readings was subtracted from the mean of the sample readings at each time point and the corrected values, along with the mean and SD were plotted using KaleidaGraph (v4.1, Synergy Software, Reading, PA). Statistical analyses on the data (*t*-test) were performed using KaleidaGraph (Biancalana & Koide, 2010, Roychaudhuri et al., 2014).

Asc1 and ASCT2 Transport Studies: D-cysteine transport experiments were performed in HEK293 cells transiently transfected with human SLC1A15 (ASCT2; Origene; Cat# RC200305) and rat SLC7A10 (Asc1; Genomics-online.com; Cat# ABIN4047848) cDNA using lipofectamine 3000 reagent. Following 72 h incubation, the cells were harvested, washed twice with HEPES buffered saline (HBS) containing 10 mM HEPES and 100 mM NaCl, counted and equal number of cells (4 x10^7 cells) distributed in tubes for each concentration of D-cysteine ranging from 0-120 μM. The cells were incubated with the different concentrations of D-cysteine at 37°C for 30 minutes. After incubation the cells were centrifuged at 3000 rpm for 5 min at RT and buffer discarded. The cells were washed 2 times with 500 μl HBS. The cells were hypotonically lysed by adding 200 μl cold sterile water to each tube and incubated at 37°C for 20 min. After hypotonic lysis 200 μl of reaction buffer (500 mM Tricine, 100 mM $MgSO_4$ and 2 mM EDTA, 1% Triton X-100 pH 7.8) containing TCEP, CHBT and K_2CO_3 was added to each tube to perform the luciferase assay to measure D-Cysteine levels in

the cells. The luciferase assay was performed as mentioned above and luminescence measured in the cell free supernates transferred to a 96 well opaque plate in a SpectraMax 96 well microplate reader and D-Cysteine levels quantified.

Nuclear Extracts Preparation: Nuclear extracts were prepared from the pancreas of age matched 6-8 weeks old WT and $SR^{-/-}$ mice as per instructions in the EpiQuik Nuclear Extraction Kit (Cat# OP-0002; Epigenetek, Farmingdale NY). The protein concentration of the samples was estimated using BCA protein assay and equal amounts of protein used in the DNMT activity assay.

DNMT Activity Assay: Total DNMT activity was measured in nuclear extracts of WT and $SR^{-/-}$ pancreas using the EpiQuik DNMT activity/inhibition assay colorimetric kit (Cat# P-3009; Epigenetek, Farmingdale NY). Equal amounts of nuclear extracts (20 μg) were added to each well of the 96 well plate and instructions followed as per the catalog. The activity of the nuclear extract was calculated as per instructions in the catalog and percent inhibition/activity plotted.

Electron Microscopy of exosomes. Plasma exosomes were imaged using transmission electron microscopy. Samples (10 μl) were adsorbed to glow discharged (EMS GloQube) ultra-thin (UL) carbon coated 400 mesh copper grids (EMS CF400-Cu-UL), by floatation for 2 min. Grids were quickly blotted then rinsed in 3 drops (1 min each) of TBS. Grids were negatively stained in 2 consecutive drops of 1% uranyl acetate with tylose (UAT), and quickly aspirated to get a thin layer of stain covering the

sample. Grids were imaged on a Hitachi 7600 TEM (or Philips CM120) operating at 80 kV with an AMT XR80 CCD (8 megapixel) camera [38].

Methyl cytosine (mC) and Hydroxymethyl cytosine (hmC) DNA Dot Blot. DNA dot blot was performed on a nitrocellulose membrane. Briefly, 200 ng of DNA was mixed with 20X SSC buffer and Milli Q water. The sample was heated at 100°C for 10 min and cooled on ice. 200 µl of 20X SSC buffer was added to the sample. The nitrocellulose membrane was pre wet in SSC buffer and applied to a 96 well vacuum manifold and washed with 20X SSC buffer and samples applied to the 96 wells of the manifold under vacuum. After the samples were adsorbed on the membrane, the membrane was placed in denaturation solution (1.5 M NaCl + 0.5 M NaOH) for 10 minutes and in neutralization solution (1M NaCl + 0.5 M Tris-Cl pH 7.0) for 5 minutes. The membrane was partially dried and placed on a filter paper wet in 20X SSC buffer and UV crosslinked in a 2400 Stratalinker in auto crosslink mode. The membrane was then incubated in blocking buffer for 30 minutes at RT with gentle shaking. After blocking the membrane was incubated with rabbit mC and hmC antibodies (1:2000 dilution) in TBST overnight at 4°C. The membrane was washed four times 15 min each in TBST and incubated with secondary antibody (1:5000 dilution) in TBST for 1 h at RT. The membrane was developed using ECL chemiluminescence on an EX ray film.

Identification and Quantitation of Nucleotides by UPLC-MRM/MS (Ultra Performance Liquid Chromatography-Multiple Reaction Monitoring/Mass Spectrometry). The identification and quantitation of nucleotides, nucleosides, nucleobases and

intermediates of IMP and UMP synthesis was performed by The Metabolomics Innovation Center (TMIC) at the University of Victoria, Proteomics Center, Canada.

Serially diluted standard solutions containing all the targeted compounds were prepared in a concentration range of 0.0005 to 50 nmol/mL in 8 % methanol. Each tissue sample was weighed into a 1.5 ml eppendorf tube. Water was added at 2 µl per mg raw material. The samples were homogenized on a MM 400 mill mixer, with the aid of two 4-mm metal balls and at a shaking frequency of 30 Hz for 1 min, three times. Methanol at 8 µl/mg was then added and the samples homogenized followed by sonication for 1 min on an ice-water bath. The samples were placed at -20°C for 2 hours and then centrifuged at 21,000 g and 5°C for 15 min. The clear supernatants were collected.

Twenty µL of the supernatant of each sample or each standard solution was mixed with 180 µL of an internal standard solution containing isotope-labeled 15N5-AMP, 13C10-ATP, 13C10-GTP, 13C5- adenosine, 15N2-adenine and 13N5-guanine. 10 µL aliquots were injected into a C_{18} column (2.1x150 mm, 1.8 µm) for UPLC-MRM/MS run on a Waters Acquity UPLC system coupled to a Sciex QTRAP 6500 Plus mass spectrometer operated in the negative-ion ESI mode for detection of nucleotides and intermediates of purine and pyrimidine synthesis. The mobile phase was tributylamine-ammonium acetate buffer (A) and acetonitrile/methanol (B) for binary gradient elution (5 % to 40 % B in 15 min), at 0.3 ml/min and 55°C.

For quantitation of nucleosides and nucleobases, 10 µl aliquots of the sample solutions and standard solutions were injected onto a polar reversed-phase C_{18} column (2.1x100 mm, 2.0 µm) to run UPLC-MRM/MS coupled to a Sciex QTRAP 6500 Plus mass spectrometer operated in the positive-ion ESI mode. The mobile phase was 0.02%

HFBA (A) and methanol (B) for binary gradient elution (0 % to 75 % B in 15 min), at 0.30 ml/min and 40°C.

Concentrations of detected analytes were calculated with internal-standard calibration by interpolating the constructed linear-regression curves of individual compounds, with the analyte- to-internal standard peak area ratios measured from the sample solutions.

cAMP Live Cell Imaging. Imaging of live HEK293 and βTC-6 cells was performed on a 3i spinning disk confocal microscope with slide chamber set up maintained at 37°C and 5 % CO_2 to maintain pH and cell viability. Image settings and parameters were controlled using Slidebook 6 software. Cells were seeded prior to imaging and transfection in 35 mm dishes with in built coverslip. Imaging was performed at 20X magnification and over 5 minutes duration with 30 second time lapse. Filter set was c562mp. For each field, 8-10 points were highlighted in the XY plane for capture. These points were based on maximal intensity of cell fluorescence in the active viewing field. Such points were highlighted in multiple fields of view. For time-lapse capture, the 8-10 points were captured at 30 second intervals for a total duration of 5 minutes. The fluorescence intensities were obtained from Image J, background subtracted and plotted versus elapsed time. Movie files were generated in Image J by combining each individual live capture file.

Chromatin Immunoprecipitation-qPCR (ChIP-qPCR). ChIP was performed from pancreas of age matched WT and $SR^{-/-}$ mice using EpiQuik tissue chromatin immunoprecipitation kit (Epigentek; #P-2003) as per instructions. Rabbit anti CREB

monoclonal antibody (Cell Signaling Technology; #D76D11) was used as per recommended dilution (1:100) to IP DNA. Following DNA elution and quantitation, 100 ng of DNA was used in qPCR reactions using the SYBR green method. Input DNA C_T values was used to subtract the C_T values from WT and $SR^{-/-}$ samples and fold change relative to WT was determined using $2^{-\Delta\Delta CT}$. IgG antibody was used as a negative control. DNMT1 promoter region (D1-D5) primer sequences used for qPCR are listed below (Zampieri et al., 2009).

D1 Reverse: 5' AAC GAG ACC CCG GCT TTT T 3'

D1 Forward: 5' TAT AGC CAG GAG GTG TGG GTG 3'

D2 Forward: 5' TCC TCT GCA AGA GCA GCA CTA 3'

D2 Reverse: 5' ATG TAC CAC ACA GGG CAA GA 3'

D3 Forward: 5' TGT TTG TGC ATG TGA GTG CA 3'

D3 Reverse: 5' TCG GCA CTT GAG AGC AGG TA 3'

D4 Forward: 5' TGA GTG CTG GAA TCA AAT GC 3'

D4 Reverse: 3' AAG CCC CTG TAA TTC CAC TT 3'

D5 Forward: 3' AGA AGT GGT TCC TGG CCT TA 3'

D5 Reverse: 3' TAA CTC TAT CCC CCT CCC CTT 3'

Acknowledgments: The authors wish to acknowledge Ms. Barbara Smith of the Microscopy Core Facility at Johns Hopkins School of Medicine for assisting on the laser scanning confocal microscope. The authors also acknowledge her assistance with live cell imaging and in obtaining electron micrographs of secretory vesicles and exosomes.

Funding: This work was supported by grant P50 DA044123 to SHS.

Author contributions: **RR** conceived the project. **RR** performed all experiments and data analysis. **RR** wrote the manuscript. **MMG** optimized the luciferase assay. **LA** did the mice genotyping. **LA** assisted **RR** in the administration and performance of glucose tolerance tests. **TW** tested the specificity of the luciferase assay towards D-cysteine. **HS** expressed and purified serine racemase using FPLC. **RR** and **SHS** edited the manuscript. All other authors reviewed the manuscript.

The authors gratefully acknowledge MMG and Mario Amzel who tragically passed away in 2018 and 2022 respectively.

Competing interests: Authors declare no competing interests.

References

Anguera MC, Field MS, Perry C, Ghandour H, Chiang EP, Selhub J, Shane B, Stover PJ (2006) Regulation of folate-mediated one-carbon metabolism by 10-formyltetrahydrofolate dehydrogenase. J Biol Chem 281: 18335-42

Bailey TS, Donor MT, Naughton SP, Pluth MD (2015) A simple bioluminescent method for measuring D-amino acid oxidase activity. Chem Commun (Camb) 51: 5425-8

Basu AC, Tsai GE, Ma CL, Ehmsen JT, Mustafa AK, Han L, Jiang ZI, Benneyworth MA, Froimowitz MP, Lange N, Snyder SH, Bergeron R, Coyle JT (2009) Targeted disruption of serine racemase affects glutamatergic neurotransmission and behavior. Mol Psychiatry 14: 719-27

Bian Y, Zheng R, Bayer FP, Wong C, Chang YC, Meng C, Zolg DP, Reinecke M, Zecha J, Wiechmann S, Heinzlmeir S, Scherr J, Hemmer B, Baynham M, Gingras AC, Boychenko O, Kuster B (2020) Robust, reproducible and quantitative analysis of thousands of proteomes by micro-flow LC-MS/MS. Nat Commun 11: 157

Biancalana M, Koide S (2010) Molecular mechanism of Thioflavin-T binding to amyloid fibrils. Biochim Biophys Acta 1804: 1405-12

Bigi A, Loffredo G, Cascella R, Cecchi C (2020) Targeting Pathological Amyloid Aggregates with Conformation-Sensitive Antibodies. Curr Alzheimer Res 17: 722-734
Corrigan JJ (1969) D-amino acids in animals. Science 164: 142-9

Dunlop DS, Neidle A (2005) Regulation of serine racemase activity by amino acids. Brain Res Mol Brain Res 133: 208-14

Pin C and Fenech M (2017) Development of the Pancreas. In Pancreapedia: Exocrine Pancreas Knowledge Base, pp 1-10. American Pancreatic Association

Fuchs SA, Berger R, Klomp LW, de Koning TJ (2005) D-amino acids in the central nervous system in health and disease. Mol Genet Metab 85: 168-80

Gao F, Liang H, Lu H, Wang J, Xia M, Yuan Z, Yao Y, Wang T, Tan X, Laurence A, Xu H, Yu J, Xiao W, Chen W, Zhou M, Zhang X, Chen Q, Chen X (2015) Global analysis of DNA methylation in hepatocellular carcinoma by a liquid hybridization capture-based bisulfite sequencing approach. Clin Epigenetics 7: 86

Genchi G (2017) An overview on D-amino acids. Amino Acids 49: 1521-1533

Harada K, Ito M, Wang X, Tanaka M, Wongso D, Konno A, Hirai H, Hirase H, Tsuboi T, Kitaguchi T (2017) Red fluorescent protein-based cAMP indicator applicable to optogenetics and in vivo imaging. Sci Rep 7: 7351

Hiratsuka T (1993) Behavior of Cys-707 (SH1) in myosin associated with ATP hydrolysis revealed with a fluorescent probe linked directly to the sulfur atom. J Biol Chem 268: 24742-50

Hutton JC, Wong R, Davidson HW (2009) Isolation of dense core secretory vesicles from pancreatic endocrine cells by differential and density gradient centrifugation. Curr Protoc Cell Biol Chapter 3: Unit 3 32

Impey S, McCorkle SR, Cha-Molstad H, Dwyer JM, Yochum GS, Boss JM, McWeeney S, Dunn JJ, Mandel G, Goodman RH (2004) Defining the CREB regulon: a genome-wide analysis of transcription factor regulatory regions. Cell 119: 1041-54

Ishii I, Kamata S, Ito S, Shimonaga A, Koizumi M, Tsushima M, Miura A, Nagata T, Tosaka Y, Ohtani H, Kamichatani W, Akahoshi N (2022) A High-Methionine Diet for One-Week Induces a High Accumulation of Methionine in the Cerebrospinal Fluid and Confers Bipolar Disorder-like Behavior in Mice. Int J Mol Sci 23

Jankowski A, Kim JH, Collins RF, Daneman R, Walton P, Grinstein S (2001) In situ measurements of the pH of mammalian peroxisomes using the fluorescent protein pHluorin. J Biol Chem 276: 48748-53

Kaplan E, Zubedat S, Radzishevsky I, Valenta AC, Rechnitz O, Sason H, Sajrawi C, Bodner O, Konno K, Esaki K, Derdikman D, Yoshikawa T, Watanabe M, Kennedy RT, Billard JM, Avital A, Wolosker H (2018) ASCT1 (Slc1a4) transporter is a physiologic regulator of brain d-serine and neurodevelopment. Proc Natl Acad Sci U S A 115: 9628-9633

Kayed R, Head E, Sarsoza F, Saing T, Cotman CW, Necula M, Margol L, Wu J, Breydo L, Thompson JL, Rasool S, Gurlo T, Butler P, Glabe CG (2007) Fibril specific, conformation dependent antibodies recognize a generic epitope common to amyloid fibrils and fibrillar oligomers that is absent in prefibrillar oligomers. Mol Neurodegener 2: 18

Khoronenkova SV, Tishkov VI (2008) D-amino acid oxidase: physiological role and applications. Biochemistry (Mosc) 73: 1511-8

Kim PM, Duan X, Huang AS, Liu CY, Ming GL, Song H, Snyder SH (2010) Aspartate racemase, generating neuronal D-aspartate, regulates adult neurogenesis. Proc Natl Acad Sci U S A 107: 3175-9

Krishnan R, Goodman JL, Mukhopadhyay S, Pacheco CD, Lemke EA, Deniz AA, Lindquist S (2012) Conserved features of intermediates in amyloid assembly determine their benign or toxic states. Proc Natl Acad Sci U S A 109: 11172-7

Lehmann J, Ye S (2019) D Amino Acids Highlight the Catalytic Power of the Ribosome. Cell Chem Biol 26: 1639-1641

Lister R, Pelizzola M, Dowen RH, Hawkins RD, Hon G, Tonti-Filippini J, Nery JR, Lee L, Ye Z, Ngo QM, Edsall L, Antosiewicz-Bourget J, Stewart R, Ruotti V, Millar AH, Thomson JA, Ren B, Ecker JR (2009) Human DNA methylomes at base resolution show widespread epigenomic differences. Nature 462: 315-22

Lockridge AD, Baumann DC, Akhaphong B, Abrenica A, Miller RF, Alejandro EU (2016) Serine racemase is expressed in islets and contributes to the regulation of glucose homeostasis. Islets 8: 195-206

Maji SK, Perrin MH, Sawaya MR, Jessberger S, Vadodaria K, Rissman RA, Singru PS, Nilsson KP, Simon R, Schubert D, Eisenberg D, Rivier J, Sawchenko P, Vale W, Riek R (2009) Functional amyloids as natural storage of peptide hormones in pituitary secretory granules. Science 325: 328-32

Man EH, Bada JL (1987) Dietary D-amino acids. Annu Rev Nutr 7: 209-25

Nelson DL, Applegate GA, Beio ML, Graham DL, Berkowitz DB (2017) Human serine racemase structure/activity relationship studies provide mechanistic insight and point to position 84 as a hot spot for beta-elimination function. J Biol Chem 292: 13986-14002

Newman JC, Verdin E (2014) Ketone bodies as signaling metabolites. Trends Endocrinol Metab 25: 42-52

Niculescu MD, Zeisel SH (2002) Diet, methyl donors and DNA methylation: interactions between dietary folate, methionine and choline. J Nutr 132: 2333S-2335S

Niwa K, Nakamura M, Ohmiya Y (2006) Stereoisomeric bio-inversion key to biosynthesis of firefly D-luciferin. FEBS Lett 580: 5283-7

Olova N, Krueger F, Andrews S, Oxley D, Berrens RV, Branco MR, Reik W (2018) Comparison of whole-genome bisulfite sequencing library preparation strategies identifies sources of biases affecting DNA methylation data. Genome Biol 19: 33

Panizzutti R, De Miranda J, Ribeiro CS, Engelender S, Wolosker H (2001) A new strategy to decrease N-methyl-D-aspartate (NMDA) receptor coactivation: inhibition of D-serine synthesis by converting serine racemase into an eliminase. Proc Natl Acad Sci U S A 98: 5294-9

Pollegioni L, Sacchi S, Murtas G (2018) Human D-Amino Acid Oxidase: Structure, Function, and Regulation. Front Mol Biosci 5: 107

Puchalska P, Crawford PA (2017) Multi-dimensional Roles of Ketone Bodies in Fuel Metabolism, Signaling, and Therapeutics. Cell Metab 25: 262-284

Raboni S, Marchetti M, Faggiano S, Campanini B, Bruno S, Marchesani F, Margiotta M, Mozzarelli A (2018) The Energy Landscape of Human Serine Racemase. Front Mol Biosci 5: 112

Rasouli M, Ostovar-Ravari A, Shokri-Afra H (2014) Characterization and improvement of phenol-sulfuric acid microassay for glucose-based glycogen. Eur Rev Med Pharmacol Sci 18: 2020-4

Reinke AA, Gestwicki JE (2011) Insight into amyloid structure using chemical probes. Chem Biol Drug Des 77: 399-411

Roychaudhuri R, Lomakin A, Bernstein S, Zheng X, Condron MM, Benedek GB, Bowers M, Teplow DB (2014) Gly25-Ser26 amyloid beta-protein structural isomorphs produce distinct Abeta42 conformational dynamics and assembly characteristics. J Mol Biol 426: 2422-41

Roychaudhuri R, Snyder SH (2022) Mammalian D-cysteine: A novel regulator of neural progenitor cell proliferation: Endogenous D-cysteine, the stereoisomer with rapid spontaneous in vitro racemization rate, has major neural roles: Bioessays: e2200002

Rutter AR, Fradley RL, Garrett EM, Chapman KL, Lawrence JM, Rosahl TW, Patel S (2007) Evidence from gene knockout studies implicates Asc-1 as the primary transporter mediating d-serine reuptake in the mouse CNS. Eur J Neurosci 25: 1757-66

Saleem F, Ametaj BN, Bouatra S, Mandal R, Zebeli Q, Dunn SM, Wishart DS (2012) A metabolomics approach to uncover the effects of grain diets on rumen health in dairy cows. J Dairy Sci 95: 6606-23

Sasamura T, Matsuda A, Kokuba Y (2002) Determination of D-amino acid oxidase activity in tumour cells. Ann Clin Biochem 39: 595-8

Sason H, Billard JM, Smith GP, Safory H, Neame S, Kaplan E, Rosenberg D, Zubedat S, Foltyn VN, Christoffersen CT, Bundgaard C, Thomsen C, Avital A, Christensen KV, Wolosker H (2017) Asc-1 Transporter Regulation of Synaptic Activity via the Tonic Release of d-Serine in the Forebrain. Cereb Cortex 27: 1573-1587

Semenza ER, Harraz MM, Abramson E, Malla AP, Vasavda C, Gadalla MM, Kornberg MD, Snyder SH, Roychaudhuri R (2021) D-cysteine is an endogenous regulator of neural progenitor cell dynamics in the mammalian brain. Proc Natl Acad Sci U S A 118

Snyder SH (2017) A Life of Neurotransmitters. Annu Rev Pharmacol Toxicol 57: 1-11

Snyder SH, Ferris CD (2000) Novel neurotransmitters and their neuropsychiatric relevance. Am J Psychiatry 157: 1738-51

Taylor BL, Liu FF, Sander M (2013) Nkx6.1 is essential for maintaining the functional state of pancreatic beta cells. Cell Rep 4: 1262-75

Tomoko Naka TI, Hisashi Hemmi, Tohru Yoshimura (2010) A highly sensitive enzymatic assay for d- and total serine detection using d-serine dehydratase from Saccharomyces cerevisiae. Journal of Molecular Catalysis B: Enzymatic 67: 150-154

Toyo'oka T, & Imai, K. (1984) New fluorogenic reagent having halogenobenzofurazan structure for thiols: 4-(Aminosulfonyl)-7-fluoro-2,1,3-benzoxadiazole. Anal Chem: 2461-2464

Tsai GE, Yang P, Chang YC, Chong MY (2006) D-alanine added to antipsychotics for the treatment of schizophrenia. Biol Psychiatry 59: 230-4

Wei J, Wu C, Lankin D, Gulrati A, Valyi-Nagy T, Cochran E, Pike VW, Kozikowski A, Wang Y (2005) Development of novel amyloid imaging agents based upon thioflavin S. Curr Alzheimer Res 2: 109-14

Wolosker H, Blackshaw S, Snyder SH (1999a) Serine racemase: a glial enzyme synthesizing D-serine to regulate glutamate-N-methyl-D-aspartate neurotransmission. Proc Natl Acad Sci U S A 96: 13409-14

Wolosker H, Sheth KN, Takahashi M, Mothet JP, Brady RO, Jr., Ferris CD, Snyder SH (1999b) Purification of serine racemase: biosynthesis of the neuromodulator D-serine. Proc Natl Acad Sci U S A 96: 721-5

Xie X, Dumas T, Tang L, Brennan T, Reeder T, Thomas W, Klein RD, Flores J, O'Hara BF, Heller HC, Franken P (2005) Lack of the alanine-serine-cysteine transporter 1 causes tremors, seizures, and early postnatal death in mice. Brain Res 1052: 212-21

Yamanaka M, Miyoshi Y, Ohide H, Hamase K, Konno R (2012) D-Amino acids in the brain and mutant rodents lacking D-amino-acid oxidase activity. Amino Acids 43: 1811-21

Zampieri M, Passananti C, Calabrese R, Perilli M, Corbi N, De Cave F, Guastafierro T, Bacalini MG, Reale A, Amicosante G, Calabrese L, Zlatanova J, Caiafa P (2009) Parp1 localizes within the Dnmt1 promoter and protects its unmethylated state by its enzymatic activity. PLoS One 4: e4717

Zeisel S (2017) Choline, Other Methyl-Donors and Epigenetics. Nutrients 9

Zhang N (2015) Epigenetic modulation of DNA methylation by nutrition and its mechanisms in animals. Anim Nutr 1: 144-151

Main Text Figure Legends (Roychaudhuri et al**)**

Figure. 1. Identification and characterization of mammalian D-cysteine. (**A**) Structure of D-cysteine (**B**) Principle of luciferase assay for bioluminescent detection of D-cysteine (figure adapted from Niwa et al., 2006 [16]). The asterisk (*) in the schematic is the chiral carbon of cysteine that corresponds to that in D-luciferin. Lower panel shows SR converting L-cysteine to D-cysteine that conjugates with CHBT to produce D-luciferin. (**C**) Amounts of L and D cysteine in the pancreas of age matched WT and $SR^{-/-}$ mice as estimated by luciferase assay (* indicates p <0.0001 value in the pancreas of $SR^{-/-}$ mice relative to WT control). (**D**) Detection of purified L and D-cysteine by chiral HPLC separation after thiol labeling by ABDF and fluorescent detection at excitation λ=380 nm and emission λ=510 nm. (**E**) HPLC estimation of L and D-cysteine in the pancreas of WT and $SR^{-/-}$ mice (* indicates p values for comparison between WT and $SR^{-/-}$ for amounts of L and D-cysteine). (**F**) *In vitro* racemization activity of recombinant purified mouse SR towards L-cysteine substrate (1 mM concentration) to produce D-cysteine measured using the luciferase assay. Amount of D-cysteine formed was quantified based on luminescence intensities from a D-cysteine standard curve. Negative control was mouse purified SR incubated with 500 mM L-cysteine (L-Cysteine is inhibitory >2 mM concentrations) and without PLP cofactor. Data are representative of 3-4 independent experiments each with different preps of recombinant purified mouse SR. (**G**) Immunohistochemistry of conjugated D-cysteine in pancreatic sections of WT and $SR^{-/-}$ mice (endocrine and exocrine). Red staining (conjugated D-cysteine) Blue (DAPI). Scale Bar=50 μ. **(H)** Confocal microscopy showing colocalization of conjugated D-cysteine with insulin in β-cells of islets in WT mice. WT mice paraffin embedded pancreatic sections were double immunostained for conjugated D-cysteine (green; Alexa 488) and insulin (red; Alexa 594). Panels show the different channels along with the merged channel.

Figure. 2. SR controls insulin secretion and islet size. (A) Insulin levels (ng/ml) in the pancreas of WT and $SR^{-/-}$ mice measured using ultrasensitive mouse insulin ELISA. Data are compiled from 3-4 independent experiments. N=12-15 mice per group. ***** p<0.001 indicates significant differences compared to age matched WT mice. **(B)** Insulin

levels (ng/ml) in the plasma of age matched WT and SR$^{-/-}$ mice measured using ELISA (as mentioned above). Data are representative of 3 independent experiments. N=12-15 mice per group. *p<0.001 indicates significant differences compared to age matched WT mice. **(C)** Glycogen levels in the liver of WT and age matched SR$^{-/-}$ mice. Glycogen was measured by phenol-sulfuric acid method [25] and absorbance read at 492 nm. Glycogen amounts in the liver homogenates were quantified based on a standard curve of purified glycogen. N=10-14 mice per genotype. Error Bars refer to SD. **(D)** Pancreatic sections from WT and SR$^{-/-}$ mice were fixed in 4% PFA in PBS, paraffin embedded, sectioned and stained with H&E dye to observe islet morphology. **(E)** Islet diameters (white arrows) were quantified using Image J in different high-powered fields and the mean islet diameters plotted for each genotype. * indicates *p* value relative to WT (*t*-test). Error Bars refer to SD. Scale Bar= 200 μm. **(F)** Total islet area (average size of each islet x total number of islets) in WT and age matched SR$^{-/-}$ mice. * indicates *p* value relative to WT (*t*-test) **(G)** Glucose tolerance test (GTT) performed in WT and age matched SR$^{-/-}$ mice. Mice were fasted for 16 h and subsequently injected intraperitoneally with 2g/kg sterile glucose prepared in sterile saline. Amount of glucose metabolized at each time point was determined by tail bleed followed by measurement of blood glucose with blood glucose strips and glucometer. Error Bars refer to SD. **(H)** Insulin levels during GTT in WT and age matched SR$^{-/-}$ mice. Insulin was estimated by ELISA at t=30 min and 120 min after i.p. injection of 2g/kg sterile glucose. Error Bars refer to SD. * indicates p value relative to WT control at the same time point. **(I)** Gene expression of pre insulin, mature insulin and glucagon in pancreas of WT and age matched SR$^{-/-}$ mice. Data are representative of 3-5 independent experiments. Error Bars refer to SD. Gene expression of **(J)** Nkx6.1 **(K)** GLUT2, Pcx and G6Pc2 **(L)** Erol1b, Slc30a8 and **(M)** Tlc3, Rfx6, MafA and Mnx1 in pancreas of age matched WT and SR$^{-/-}$ mice. Realtime PCR was performed using SYBR green protocol on an ABI Step One Plus thermocycler. Data are representative of 3 independent experiments.

Figure. 3. Excess insulin stored as functional amyloid in secretory vesicles and exosomes (A) Dot blot of plasma exosomes isolated from WT and SR$^{-/-}$ mice plasma and probed using OC antibody (1:1000 dilution) (generic antibody for fibrillar

aggregates). Data are representative of 3 independent experiments. **(B)** IHC colocalization of insulin and amyloid aggregates in islets of WT and age matched $SR^{-/-}$ mice. Insulin staining (red), amyloid staining (green) and merged (yellow) imaged using laser scanning confocal microscopy. Scale Bar= 50 μ. **(C)** Dot blot of secretory vesicles isolated from WT and SR#8 βTC-6 cells probed for insulin using mouse insulin antibody. Blot is representative of 3 independent experiments **(D)** TEM images of plasma exosomes from WT and $SR^{-/-}$ mice following staining by uranyl acetate [38]. Numbers on the image (white highlight) indicate diameter of exosome. **(E)** Dot blot of secretory vesicles isolated from WT and SR#8 βTC-6 cells probed for amyloid using OC antibody [32-34]. Blot is representative of 3 independent experiments. **(F)** Plasma exosome size distribution. Exosomes from plasma of WT and age matched $SR^{-/-}$ mice were isolated and imaged using transmission electron microscopy. Exosome size was quantified in the different high-powered fields using Image J and plotted. Statistical analyses were performed (student *t*-test) and *p* values obtained. ***** p=0.00012 relative to WT. **(G)** ThT fluorescence assay time course of plasma exosomes from isolated from WT and $SR^{-/-}$ mice following exosome lysis. Fluorescence was measure at ex λ 450 nm and em λ 490 nm. Error Bars refer to SD. * p=0.0063 indicates difference in fluorescence intensity between WT and $SR^{-/-}$ samples at the end of the time course. Data are representative of 3-4 independent experiments. **(H)** Thioflavin T (ThT) Fluorescence of βTC-6 isolated secretory vesicles. Secretory vesicles from WT and SR knockdown cells (SR#8) were harvested and lysed by sonication. Equal amounts of protein were added to each well of a 96 well plate along with 1 mM ThT in PBS. The plate was incubated at 37°C for 24 h without shaking and read after 24 h in a microplate reader at ex λ = 450 nm and em λ = 482 nm. PBS containing ThT was used as blank. Blank mean fluorescence was used to subtract the readings from WT and SR#8. The corrected values along with the mean and SD were plotted using KaleidaGraph. Statistical analyses on the data (*t*-test) were performed in KaleidaGraph. ***** indicates p<0.0001 compared to WT sample. **(I)** Thioflavin S staining in islets. Islets of 6-8 weeks old WT and $SR^{-/-}$ mice were stained with Thioflavin S to determine the presence of amyloid aggregates. Thioflavin S positive staining (green dots) in the islets show the presence of

amyloid aggregates. Images were captured on laser scanning LSM 800 confocal microscope. Scale Bar= 20 μm.

Figure. 4. SR controls nucleotide metabolism in the pancreas. (A) Manhattan plot of global proteomic analysis in pancreas of WT and $SR^{-/-}$ mice by nano LC-MS/MS. Fold change was deemed significant above or below 1.5. The names of the top ten proteins are listed above their gene symbols in the Manhattan plot. All proteins are identified in table 4. Estimation of **(B)** AMP *p<0.001 relative to WT control, **(C)** ADP *p<0.001 relative to WT control, **(D)** ATP **(E)** GMP **(F)** GDP **(G)** GTP **(H)** dGTP **(I)** IMP **(J)** IDP **(K)** ITP **(L)** CTP **(M)** TMP in WT and $SR^{-/-}$ pancreas by UPLC-MRM-MS. Data are obtained from analysis of samples comprising of 5-8 mice per group. Concentration on y axis are nmoles/gram of tissue. Error bars refer to SD and statistics (*p* values) was performed using student *t* test in KaleidaGraph. G=Guanosine, A=Adenosine, I=Inosine, C=Cytosine, T=Thymidine.

Figure. 5. D-Cysteine signals via a cyclic AMP dependent mechanism. (A) Cyclic AMP levels in WT and $SR^{-/-}$ pancreatic supernates estimated by ELISA *p<0.001 relative to WT control. N=5-8 mice samples were pooled and analyzed in quadruplicate. Error Bars refer to SD. **(B)** Immunohistochemistry of exocrine and islets of WT and $SR^{-/-}$ mice for cAMP expression. Sections were stained with 1:500 dilution of anti-mouse cAMP antibody followed by anti-mouse secondary antibody Alexa 594. Arrows indicate boundary of islet (bottom panel). Scale Bar=100 μ. **(C)** Snapshot of live cell imaging of βTC-6 cells transfected with cAMP sensor pink flamindo and treated with 50 mM forskolin, L-cysteine and D-cysteine. Fluorescence was measured at 20X using idisk spinning confocal microscopy at 562 nm wavelength. Scale Bar=100 μ **(D)** Quantitative analysis of mean fluorescence intensities at each elapsed time point in the live cell imaging process at one position. Data were obtained and processed using Slidebook 6 (digital microscopy software). **(E)** Schematic of mode of action of endogenous D-cysteine.

Figure. 6. SR controls global and *Ins1* promoter methylation. (A) Expression of CREB and p-CREB (S133) in pancreatic lysates of WT and $SR^{-/-}$ mice. Equal amounts of protein were loaded on a gel. Samples are pooled from 5-10 mice and run in duplicate. Data are representative of 3-5 independent experiments. **(B)** Expression of CREB and p-CREB (S133) in pancreatic nuclear lysates of WT and $SR^{-/-}$ mice. Nuclear lysates were prepared from nuclear fractionation kit (EpiQuik nuclear extraction kit; Epigentek) and purity assessed by probing with laminin A/C (nuclear fraction) and β-tubulin (cytoplasmic fraction). Equal amounts of protein were loaded on a gel. Samples are pooled from 5-10 mice and run in duplicate. Data are representative of 3-5 independent experiments. Laminin A/C was a nuclear loading control. **(C)** Predicted CpG islands in *Ins1* promoter. GC content (red). Green line indicates CpG observed/expected value. CpG islands (yellow) around position 2500 in the *Ins1* promoter. The highlighted region (yellow) was analyzed by bisulfite sequencing PCR to determine methylation levels in WT and $SR^{-/-}$ pancreas. **(D-E)** Global methyl cytosine (mC) and hydroxymethyl cytosine (hmC) expression in WT and $SR^{-/-}$ pancreas following DNA dot blot on a nitrocellulose membrane and probed with mouse monoclonal mC and hmC antibody (1:2000 dilution) respectively. Data are representative of 3 independent experiments. **(F)** Whole genome bisulfite sequencing of *Ins1* promoter of WT and $SR^{-/-}$ mice (around region 2500 of *Ins1* promoter). Data show CpG methylation at 7 different CpG sites. p values indicate differences between WT and $SR^{-/-}$ *Ins1* promoter at the different methylation sites. **(G)** Expression of DNMT1, DNMT3A and DNMT3B in pancreatic nuclear extracts of WT and $SR^{-/-}$ mice. Nuclear extracts were prepared as mentioned above (and in methods). Equal amounts of protein were loaded on a gel. Samples are pooled from 5-10 mice and run in duplicate. Data are representative of 3-5 independent experiments. Laminin A/C was a nuclear loading control. Lower sized arrows indicate processed forms of DNMT3A and DNMT3B. **(H)** Schematic of the promoter region of DNMT1 gene and CREB occupancy in the pancreas of WT and $SR^{-/-}$ mice. D1-D5 indicate the different regions on the promoter that were analyzed following ChIP with CREB antibody for fold change in DNMT1 expression in real time PCR using SYBR green method. Numbers designate regions upstream of the transcription start site (dark arrow). **(I)** Total DNMT activity in nuclear extracts of pancreas of age matched WT

and $SR^{-/-}$ mice. Nuclear extracts were prepared from pancreas (as mentioned) and equal amounts of protein (20 μg) was added to each well of a total DNMT activity assay 96 well plate (Epigentek). The percent reduction in total DNMT activity was measured relative to WT. * p <0.0001 indicates significance relative to WT control. **(J)** ChIP-qPCR of region D1-D5 of *DNMT1* promoter immunoprecipitated with CREB antibody. Region D1-D5 span the promoter region of DNMT1 including 183 bases into exon1 (D5). Fold change in expression of the promoter regions are indicated relative to WT control. Region D3 (214 bp) was not plotted as it did not show any change in expression.

Figure. 7. Methyl donor dietary supplementation rescues excess insulin and DNMT activity. (A) Schematic of methionine and SAM from dietary supplementation coupled with folate cycle **(B)** Estimation of insulin in the pancreas and plasma of WT and $SR^{-/-}$ mice fed normal (0.4 % methionine) and or a high carbohydrate diet containing 0.8 % methionine (higher methyl donor) for 6 months. Insulin was measured using ultrasensitive mouse insulin ELISA kit (Crystal Chem). Samples for estimation were pooled from a total of N=10-12 mice per group per genotype and assessed in triplicate-quadruplicate in ELISA. * p <0.0001 indicates significance relative to WT control for normal and high carb diet. **(C)** DNA dot blot of global mC and hmC expression in the pancreas of WT and $SR^{-/-}$ mice fed normal (0.4 % methionine) and or a high carb diet containing 0.8 % methionine (higher methyl donor) for 6 months. **(D)** Estimation of insulin in the plasma of WT and $SR^{-/-}$ mice fed normal (0.4 % methionine) and or a high carbohydrate diet containing 0.8 % methionine (higher methyl donor) for 6 months. **(E)** Total DNMT activity in nuclear extracts of mice fed normal (0.4 % methionine) and or a high methyl donor diet containing 1.18 % methionine (high methyl donor) for 3 months. Percent activity was measured using total DNMT activity assay kit (Epigentek) as per instructions. * p <0.001 indicates significance relative to WT control among the groups. **(F)** Estimation of insulin in the pancreas of WT and $SR^{-/-}$ mice fed normal (0.4 % methionine) and or a high methyl donor diet (1.18 % methionine) for 3 months. Insulin was measured as mentioned above. Samples for estimation were pooled from a total of N=10-12 mice per group per genotype and assessed in triplicate-quadruplicate in ELISA. * p <0.0001 indicates significance relative to WT control for normal and high

methyl donor diet groups. (**G**) Phosphorylation of CREB (S133) in pancreatic lysates of WT and $SR^{-/-}$ mice fed a regular (0.5 % methionine) and or methyl donor diet (1.18% methionine) for 3 months ad libitum. Actin was a loading control.

Figure. 8. Endogenous D-cysteine is transported by ASCT2 and Asc1. (**A**) HEK293 cells were transfected with ASCT2 and treated with different concentrations of D-cysteine (x axis) for 30 minutes at 37°C. Cells were harvested, washed and lysed and D-cysteine levels measured using luciferase assay. Data show levels of intracellular D-cysteine indicated by luminescence (y axis). (**B**) HEK293 cells were transfected with Asc-1 and treated with exogenous D-cysteine for 30 minutes at 37°C. Cells were harvested, washed and lysed and D-cysteine concentration measured using luciferase assay. Data show levels of intracellular D-cysteine indicated by luminescence. (**C**) Litter mate WT, Asc1 $^{+/-}$ and Asc1 $^{-/-}$ pups (10 day old) pancreas were harvested. Samples were pooled homogenized and sonicated to extract free endogenous D-cysteine and supernatants assayed using luciferase assay. Luminescence was measured in the supernatant samples and D-cysteine concentrations obtained from standard curve. Each genotype had N=10-12 mice. Data are representative of 3 independent experiments. (**D**) Pancreatic and liver lysates of WT and age-matched $Asc1^{-/-}$ pups (litter mates) showing expression of SR. Actin was a loading control. **(E)** Schematic of D-cysteine transport in HEK293 cells by ASCT2 and Asc1 transporters.

Supplemental Figure Legends and Tables.

Figure. S1. Luciferase assay of thiol containing small molecules. **(A)** Standard curve of D-cysteine in rabbit pancreatic lysates using the luciferase assay. Standard curve was used for estimation of D-cysteine in the pancreas of mice and in βTC-6 cells. Error Bars represent SD. **(B)** Luciferase assay was performed on the different thiol containing small molecules similar to D-Cysteine and D-serine to determine specificity of the luciferase assay for D-cysteine. Five μM concentrations of D-cysteine, cysteamine, L-homocysteine, D-homocysteine, homocysteine thiolactone, L-glutathione, D-serine, L-serine and L-cysteine were assayed to determine specificity of the luciferase assay. Plot shows luminescence of the D-cysteine and the different small molecules.

Each sample was assayed in triplicate and a minimum of 3 independent experiments. Error Bars represent SD.

Figure. S2. Knockdown of SR in βTC-6 cells. (A) βTC-6 cells were treated with shRNA lentivirus particles for SR gene. Viral particles #5 and #8 refer to particles targeting different regions of SR gene. Control βTC-6 cells received pLKO.1 with scrambled viral particles. Expression of SR was determined by western blot of βTC-6 cell lysates using a rabbit polyclonal SR antibody. Actin was a loading control. **(B)** Plot shows levels of D-cysteine in βTC-6 cells measured using luciferase assay. SR#8 refer to βTC-6 cells knockdown with lentiviral particle #8 (above). SR#8 βTC-6 cells were used in our experiments.

Figure. S3. Conjugated D-cysteine immunohistochemistry in WT mice eye. (A) Localization of conjugated D-cysteine in the eyes of 8 weeks and 12 month old WT mice. Inset shows magnified image in 12 month old eye section. **(B**) Conjugated D-cysteine levels in the eyes of $SR^{-/-}$ mice at 8 weeks old (negative control). Scale Bar=20 μm. **(C)** Comparison of D-cysteine levels in eyes of 6 weeks old and 12 month old WT mice by luciferase assay. N=8-10 mice per group. (* indicates $p<0.0001$ compared to 6 weeks old mice measured using ANOVA in Kaleida Graph software).

Figure. S4. Co localization of insulin and amyloid aggregates in βTC-6 cells. WT (top panel) and SR#8 (SR knockdown; bottom panel) βTC-6 cells were grown to 70 % confluency on coverslips, fixed in 4 % PFA in PBS and stained with mouse OC antibody (amyloid; green; Alexa 488) and insulin (red; Alexa 594) to determine storage of insulin in the secretory granules. Merged panel (extreme right panels) shows colocalization of insulin and amyloid aggregates in the secretory vesicles of βTC-6 cells. Scale Bar= 10 μm.

Figure. S5. Global Proteomic Analysis (downregulated proteins). Fold change (decrease) in protein expression (Y-axis) in pancreatic lysates of WT and $SR^{-/-}$ (SRKO) mice following nano LC-MS/MS analysis. Data was quantified using Maxquant (1.6.2.6)

against a mouse database. Fold change was deemed significant when quantitative ratios were above 1.5 or below 1.5. Complete list of proteins (on X-axis) is shown in Table 4.

Figure. S6. Live cell imaging of HEK293 cells. Imaging intracellular cAMP in live HEK293 cells upon treatment with 50 μM Forskolin, 50 μM L and D-Cysteine for 24 h at 37°C. Control panel was untreated. Images are random snapshots of live cell imaging performed with 3i spinning disk confocal microscope. HEK293 cells were transfected with intracellular cAMP sensor "pink flamindo" (pink fluorescent cAMP indicator) (ex λ=560 nm and em λ=610 nm) and imaged 48 h post transfection [46]. Imaging was performed over a duration of 5 minutes at 30 second interval for each cell treatment at 37°C. Panel on the right shows mean fluorescence intensities at one position (snapshot) during the live imaging versus elapsed time (seconds). Data were obtained and processed using Slidebook 6 (digital microscopy software). Scale bar =100 μ.

Figure. S7. Nucleotide analysis by UPLC-MRM-MS. Amounts of TTP and dIMP in the pancreas of WT and $SR^{-/-}$ mice. Data are obtained from analysis of samples comprising an N of 5-8 mice per group. Concentration on y axis is nmoles/gram of tissue. Error bars refer to SD and statistics (*p* values) was performed using student *t* test in KaleidaGraph.

Figure. S8. Body weights and metabolic parameters of $SR^{-/-}$ mice. (**A**) Plasma fasting insulin levels in age matched WT and $SR^{-/-}$ mice. N=5-8 mice per genotype were sampled for isolation of plasma.* indicates p value relative to WT control mice. (**B**) Weights of WT and age matched $SR^{-/-}$ mice fed a normal and or a high carbohydrate diet (0.8% methionine) for 6 months. N=6-12 mice per group. * indicates p value relative to WT control compared to the same group of mice.

Figure. S9. Colocalization of endogenous D-cysteine and insulin in exocrine pancreas of WT mouse (**A**) Confocal microscopy of conjugated D-cysteine expression (green; Alexa 488) in the exocrine pancreas of WT mice. Insulin (red; Alexa 594) was a

negative control. DAPI was a nuclear stain. Scale Bar=20μ. **(B)** Expression of SR in islets and exocrine pancreas of WT mice (6-8 weeks old). Scale Bar=50 μ.

Figure. S10. Insulin expression in WT and SR$^{-/-}$ mouse islets. Insulin expression in islets of WT and SR$^{-/-}$ mice was detected by staining paraffin embedded pancreatic sections with rabbit polyclonal insulin antibody (1:1000 dilution) and goat anti rabbit-Alexa 594 secondary antibody (1:2000 dilution). DAPI was used as a nuclear stain. Images were captured on laser scanning LSM 800 confocal microscope. Scale Bar = 100 μm.

Tables.

Table 1. Kinetics of racemization by Serine Racemase. Table shows summary of kinetic parameters of racemization reaction of SR towards L-serine and L-cysteine to produce D-serine and D-cysteine respectively in a PLP dependent reaction followed by breakdown of generated D-serine and D-cysteine by D amino acid oxidase (DAO) and horseradish peroxidase. The peroxide produced was measured by Amplex Red fluorescence [23]. Data are mean of 4 different purified preps of recombinant mouse SR.

Table 2. Estimation of ketone bodies in liver of WT and SR$^{-/-}$ mice by ^{1}H-NMR. Ketone bodies were estimated by chloroform fractionation method. ^{1}H NMR spectra was acquired on a Bruker Avance Ascend 700 MHz spectrometer at 25°C. Amounts of the different ketone bodies were quantified based on added dimethyl silapentane sulfonate (DSS) chemical shift referencing standard. The amount of ketone bodies is listed in micrograms per gram of liver tissue [26].

Table 3. Kinetics of degradation of D-serine and D-cysteine by purified porcine D-amino acid oxidase (DAO). Equimolar amounts of substrates were incubated with purified DAO at 37°C in presence of FAD and NADPH in 0.1 M Tris-Cl pH 7.5 buffer to produce ammonia and α-ketoglutarate. In presence of glutamate dehydrogenase, the ammonia and α-ketoglutarate form L-glutamate coupled with the oxidation of NAD(P)H to NAD(P)$^{+}$; the latter conversion corresponds to the ammonia concentration and is

measured by monitoring the decrease in absorbance at 340 nm. SD refers to standard deviation.

Table 4. Complete list of proteins in the pancreas of WT and SR$^{-/-}$ mice identified in a proteomic analysis by LC-MS/MS. List of proteins identified in a quantitative label free LC-MS/MS screen with protein ID, protein name, gene name, MS ionization intensities and fold change KO/WT. Column J (last) indicates up or down regulation in SR$^{-/-}$ relative to WT of proteins.

Table 5. List of primer sequences of genes used in this study by SYBR Green method.

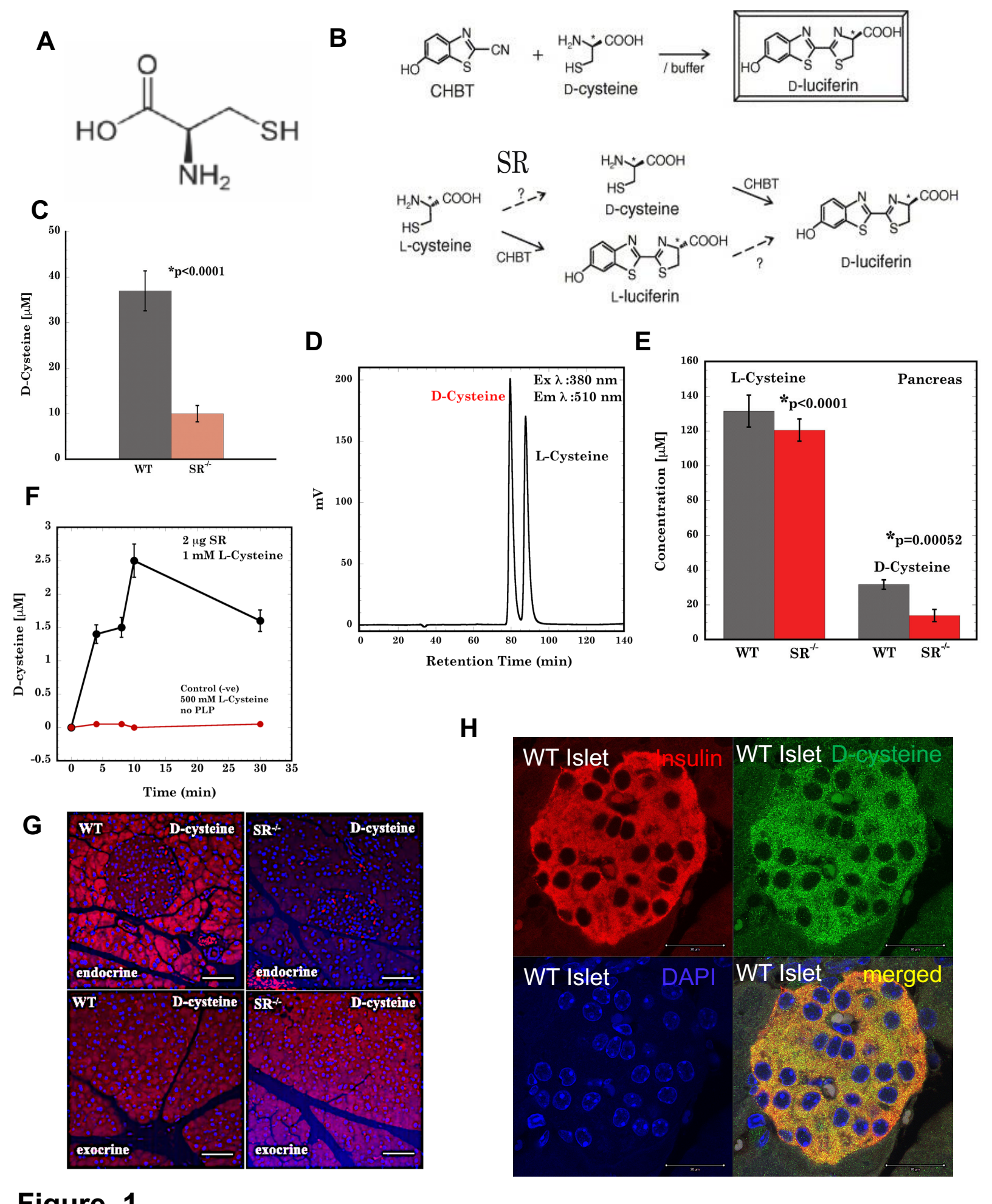
A
HO
O
SH
NH2
B
CHBT
D-cysteine
/ buffer
D-luciferin
SR
L-cysteine
L-luciferin
CHBT
C
*p<0.0001
D-Cysteine [μM]
WT
SR-/-
D
D-Cysteine
Ex λ :380 nm
Em λ :510 nm
L-Cysteine
mV
Retention Time (min)
E
L-Cysteine
Pancreas
*p<0.0001
*p=0.00052
D-Cysteine
Concentration [μM]
WT
SR-/-
WT
SR-/-
F
2 μg SR
1 mM L-Cysteine
Control (-ve)
500 mM L-Cysteine
no PLP
D-cysteine [μM]
Time (min)
G
WT
D-cysteine
SR-/-
D-cysteine
endocrine
exocrine
H
WT Islet
Insulin
WT Islet
D-cysteine
WT Islet
DAPI
WT Islet
merged

Figure. 1

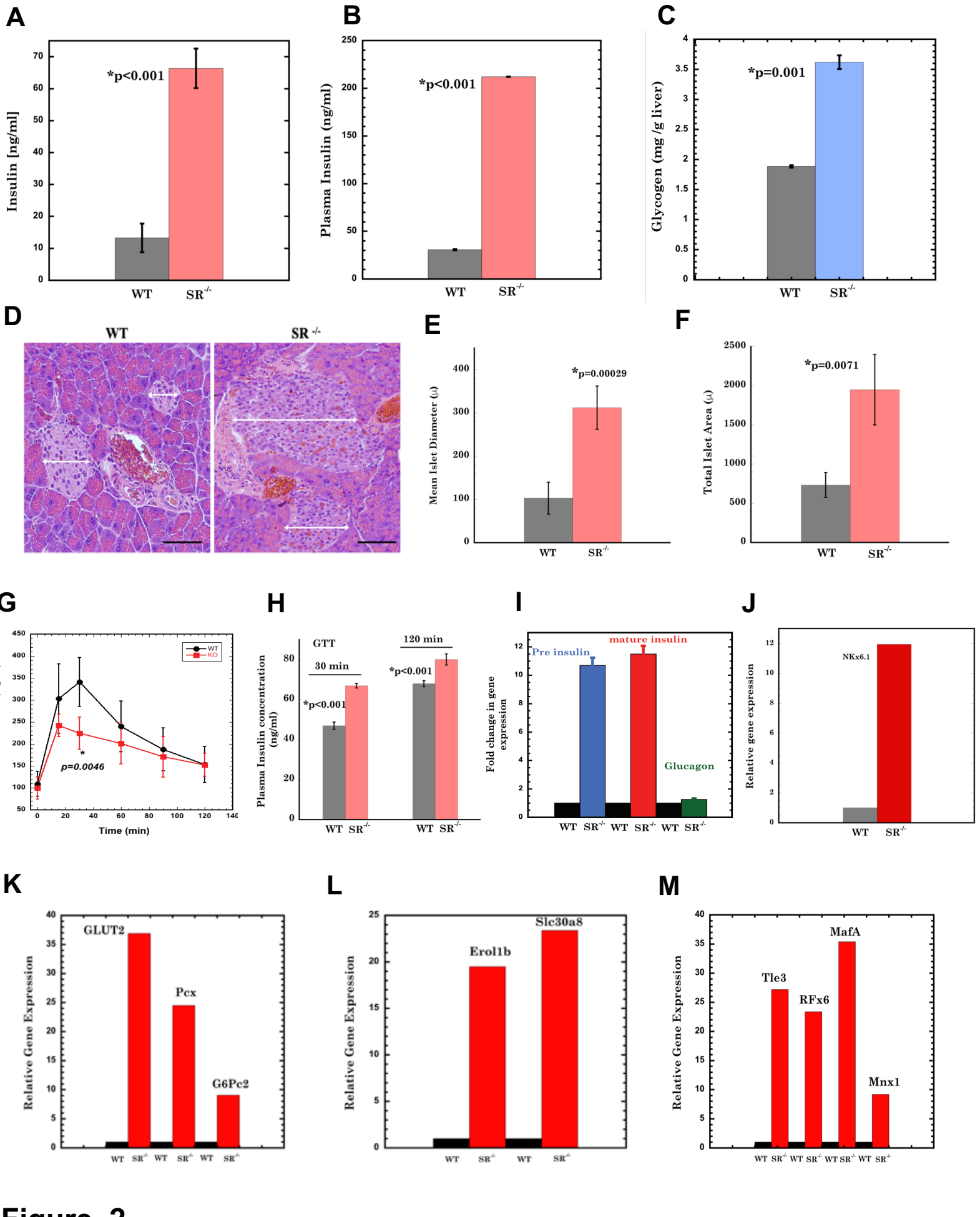
A
Insulin [ng/ml]
*p<0.001
WT
SR-/-
B
Plasma Insulin (ng/ml)
*p<0.001
WT
SR-/-
C
Glycogen (mg /g liver)
*p=0.001
WT
SR-/-
D
WT
SR -/-
E
Mean Islet Diameter (μ)
*p=0.00029
WT
SR-/-
F
Total Islet Area (μ)
*p=0.0071
WT
SR-/-
G
Amount of Glucose (mg/dL)
WT
KO
*
p=0.0046
Time (min)
H
GTT
30 min
120 min
*p<0.001
*p<0.001
Plasma Insulin concentration (ng/ml)
WT SR-/- WT SR-/-
I
Fold change in gene expression
Pre insulin
mature insulin
Glucagon
WT SR-/- WT SR-/- WT SR-/-
J
Relative gene expression
NKx6.1
WT
SR-/-
K
Relative Gene Expression
GLUT2
Pcx
G6Pc2
WT SR-/- WT SR-/- WT SR-/-
L
Relative Gene Expression
Slc30a8
Erol1b
WT
SR-/-
WT
SR-/-
M
Relative Gene Expression
MafA
Tle3
RFx6
Mnx1
WT SR-/- WT SR-/- WT SR-/- WT SR-/-

Figure. 2

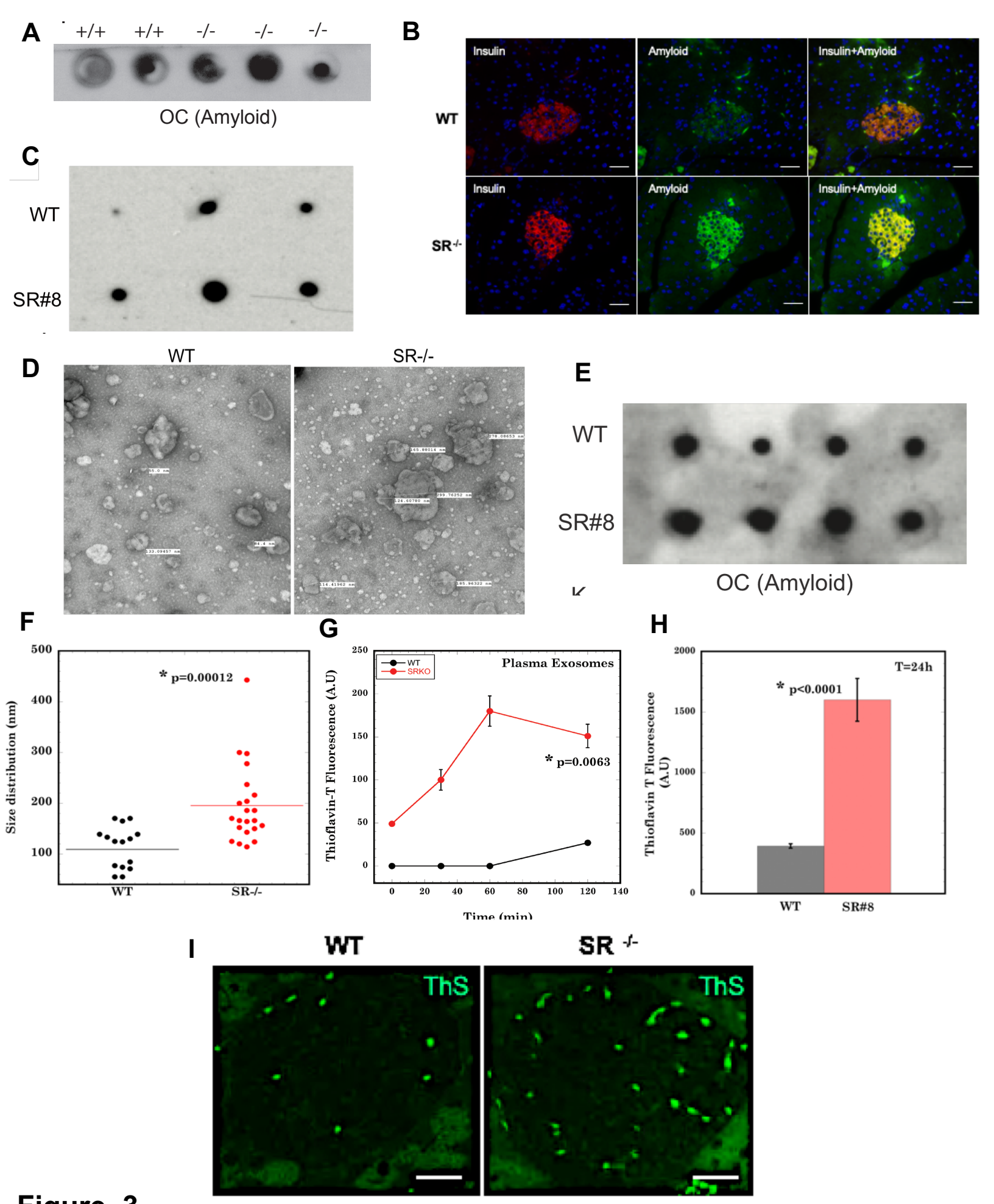
A
+/+ +/+ -/- -/- -/-
OC (Amyloid)
B
Insulin
Amyloid
Insulin+Amyloid
WT
SR-/-
C
WT
SR#8
D
WT
SR-/-
E
WT
SR#8
OC (Amyloid)
F
* p=0.00012
Size distribution (nm)
WT
SR-/-
G
Plasma Exosomes
WT
SRKO
* p=0.0063
Thioflavin-T Fluorescence (A.U)
Time (min)
H
T=24h
* p<0.0001
Thioflavin T Fluorescence (A.U)
WT
SR#8
I
WT
SR -/-
ThS
ThS

Figure. 3

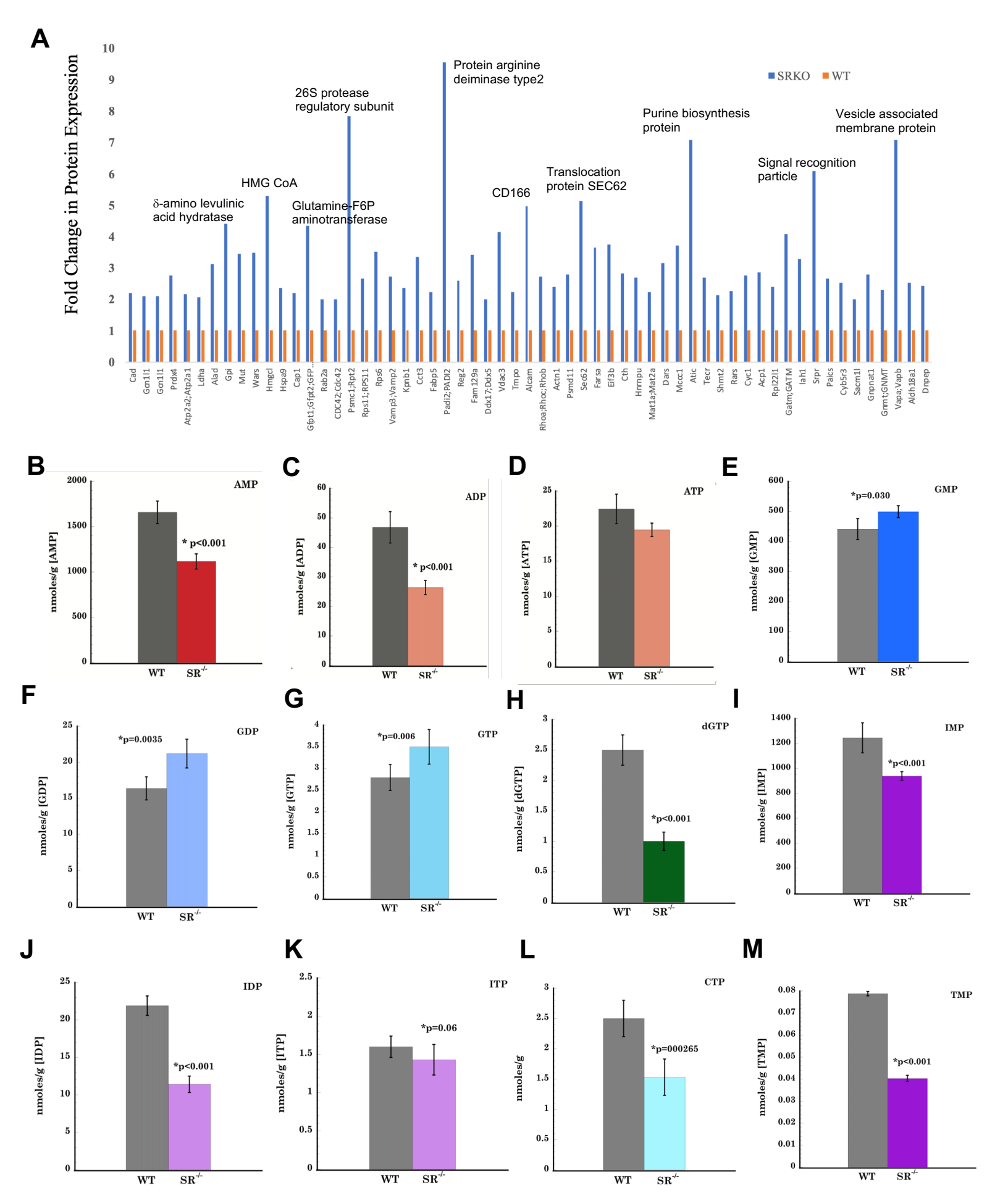
A
Fold Change in Protein Expression
SRKO
WT
δ-amino levulinic acid hydratase
HMG CoA
Glutamine-F6P aminotransferase
26S protease regulatory subunit
Protein arginine deiminase type2
CD166
Translocation protein SEC62
Purine biosynthesis protein
Signal recognition particle
Vesicle associated membrane protein
B
AMP
* p<0.001
C
ADP
* p<0.001
D
ATP
E
GMP
*p=0.030
F
GDP
*p=0.0035
G
GTP
*p=0.006
H
dGTP
*p<0.001
I
IMP
*p<0.001
J
IDP
*p<0.001
K
ITP
*p=0.06
L
CTP
*p=000265
M
TMP
*p<0.001
WT
SR-/-

Figure. 4

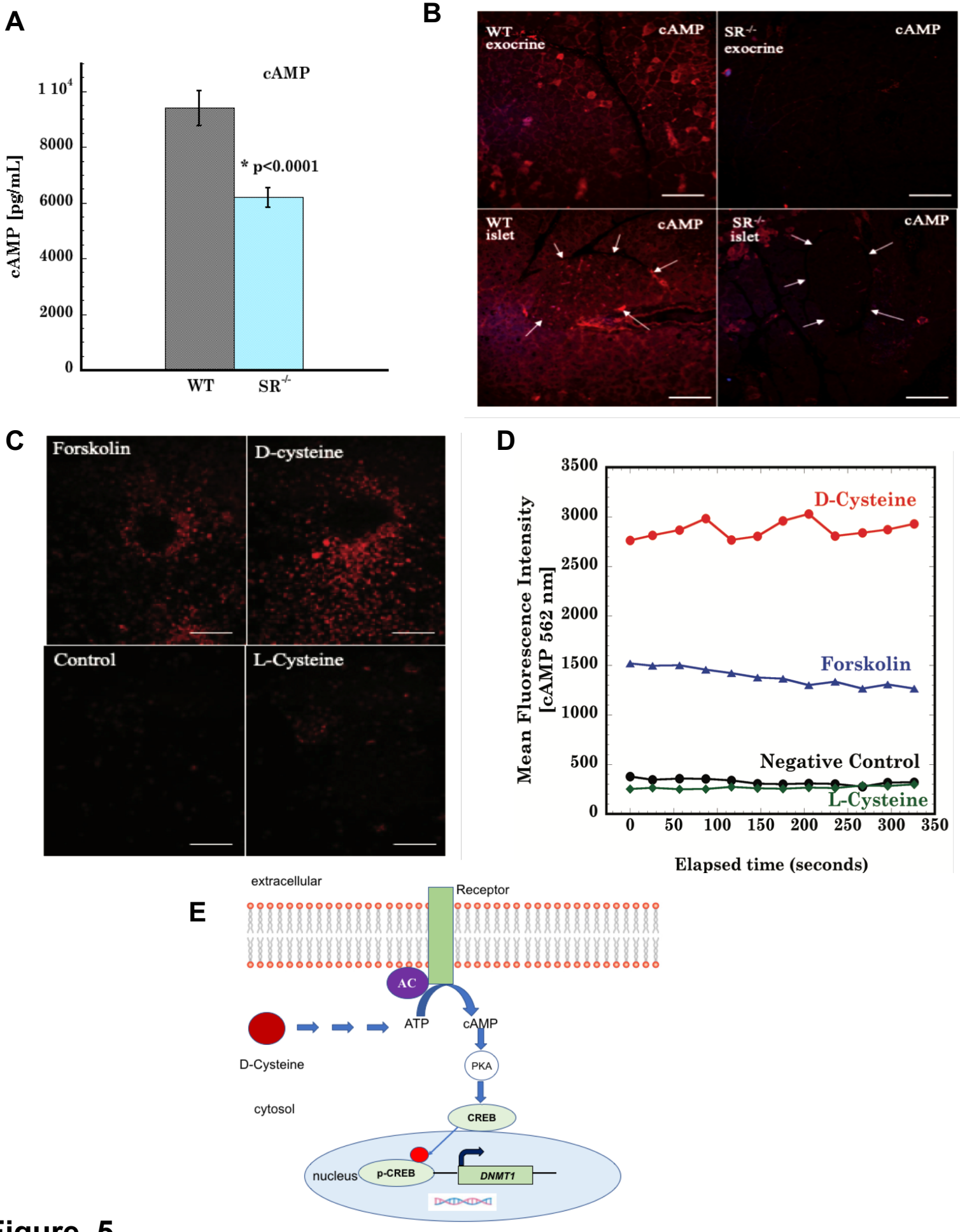
A
cAMP
cAMP [pg/mL]
1 10^4
8000
6000
4000
2000
0
* p<0.0001
WT
SR-/-
B
WT exocrine
cAMP
SR-/- exocrine
cAMP
WT islet
cAMP
SR-/- islet
cAMP
C
Forskolin
D-cysteine
Control
L-Cysteine
D
Mean Fluorescence Intensity [cAMP 562 nm]
3500
3000
2500
2000
1500
1000
500
0
D-Cysteine
Forskolin
Negative Control
L-Cysteine
0
50
100
150
200
250
300
350
Elapsed time (seconds)
E
extracellular
Receptor
AC
ATP
cAMP
D-Cysteine
PKA
cytosol
CREB
nucleus
p-CREB
DNMT1

Figure. 5

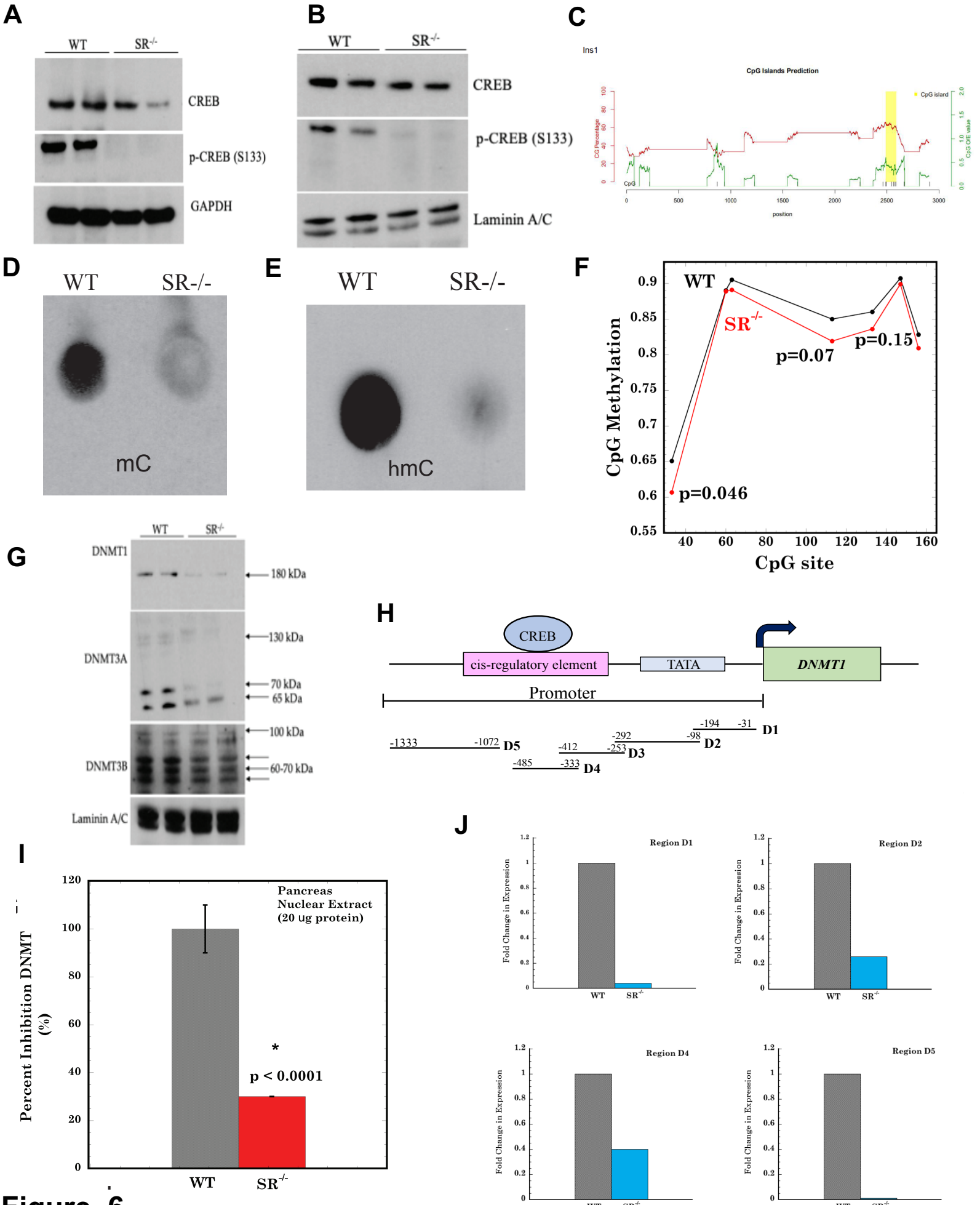
A
WT
SR-/-
CREB
p-CREB (S133)
GAPDH
B
WT
SR-/-
CREB
p-CREB (S133)
Laminin A/C
C
Ins1
CpG Islands Prediction
CpG island
CG Percentage
CpG O/E value
CpG
position
D
WT
SR-/-
mC
E
WT
SR-/-
hmC
F
WT
SR-/-
p=0.07
p=0.15
p=0.046
CpG Methylation
CpG site
G
WT
SR-/-
DNMT1
180 kDa
DNMT3A
130 kDa
70 kDa
65 kDa
DNMT3B
100 kDa
60-70 kDa
Laminin A/C
H
CREB
cis-regulatory element
TATA
DNMT1
Promoter
-194
-31
D1
-1333
-1072
D5
-292
-98
D2
-412
-253
D3
-485
-333
D4
I
Pancreas
Nuclear Extract
(20 ug protein)
Percent Inhibition DNMT (%)
*
p < 0.0001
WT
SR-/-
J
Region D1
Region D2
Region D4
Region D5
Fold Change in Expression
WT
SR-/-

Figure. 6

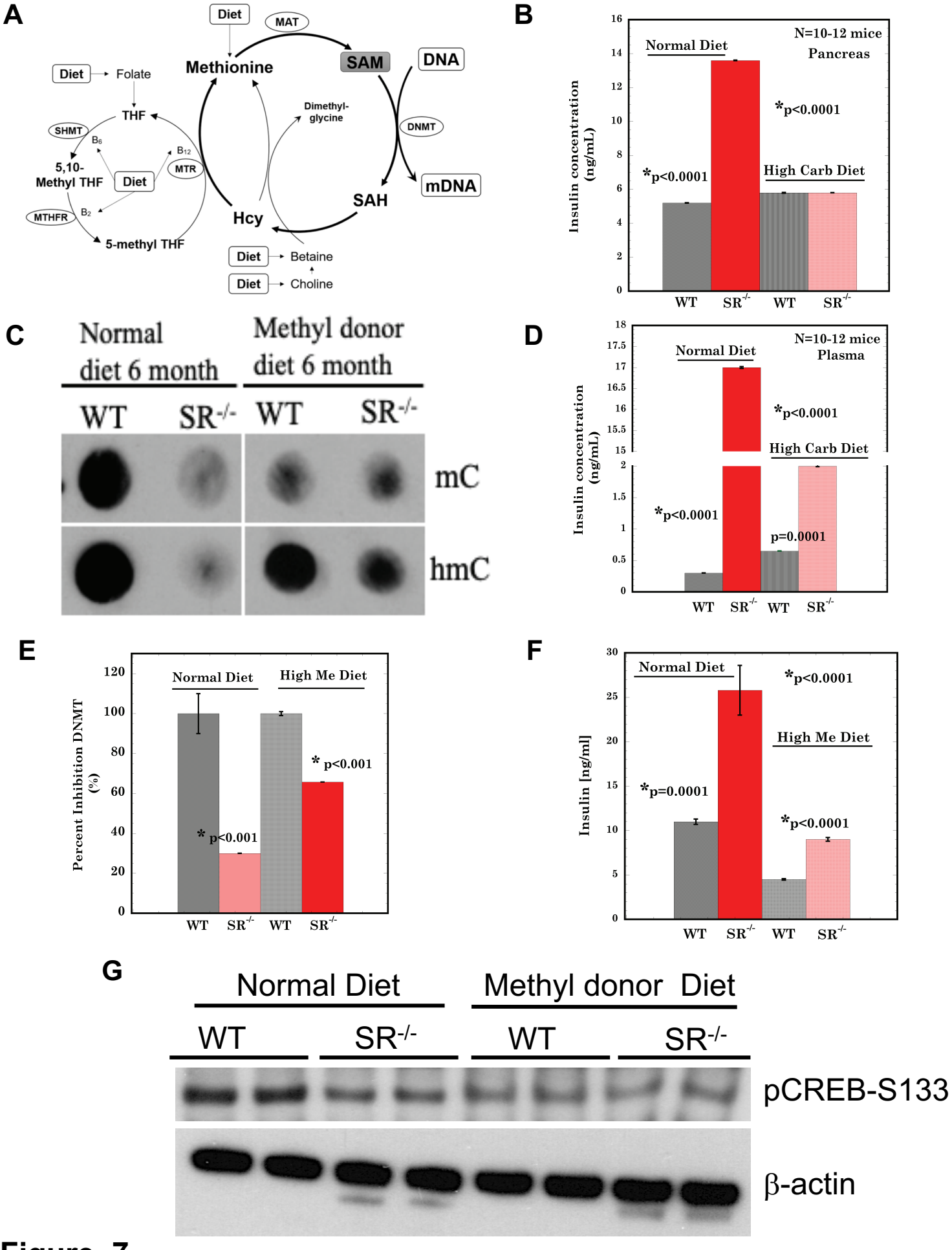
A
Diet
MAT
Methionine
SAM
DNA
Diet
Folate
THF
SHMT
B6
B12
MTR
5,10-
Methyl THF
Diet
MTHFR
B2
5-methyl THF
Dimethyl-
glycine
DNMT
mDNA
SAH
Hcy
Diet
Betaine
Diet
Choline
B
N=10-12 mice
Pancreas
Normal Diet
*p<0.0001
*p<0.0001
High Carb Diet
Insulin concentration
(ng/mL)
WT
SR-/-
WT
SR-/-
C
Normal
diet 6 month
Methyl donor
diet 6 month
WT
SR-/-
WT
SR-/-
mC
hmC
D
N=10-12 mice
Plasma
Normal Diet
*p<0.0001
High Carb Diet
*p<0.0001
p=0.0001
Insulin concentration
(ng/mL)
WT
SR-/-
WT
SR-/-
E
Normal Diet
High Me Diet
* p<0.001
* p<0.001
Percent Inhibition DNMT
(%)
WT
SR-/-
WT
SR-/-
F
Normal Diet
*p<0.0001
High Me Diet
*p=0.0001
*p<0.0001
Insulin [ng/ml]
WT
SR-/-
WT
SR-/-
G
Normal Diet
Methyl donor Diet
WT
SR-/-
WT
SR-/-
pCREB-S133
β-actin

Figure. 7

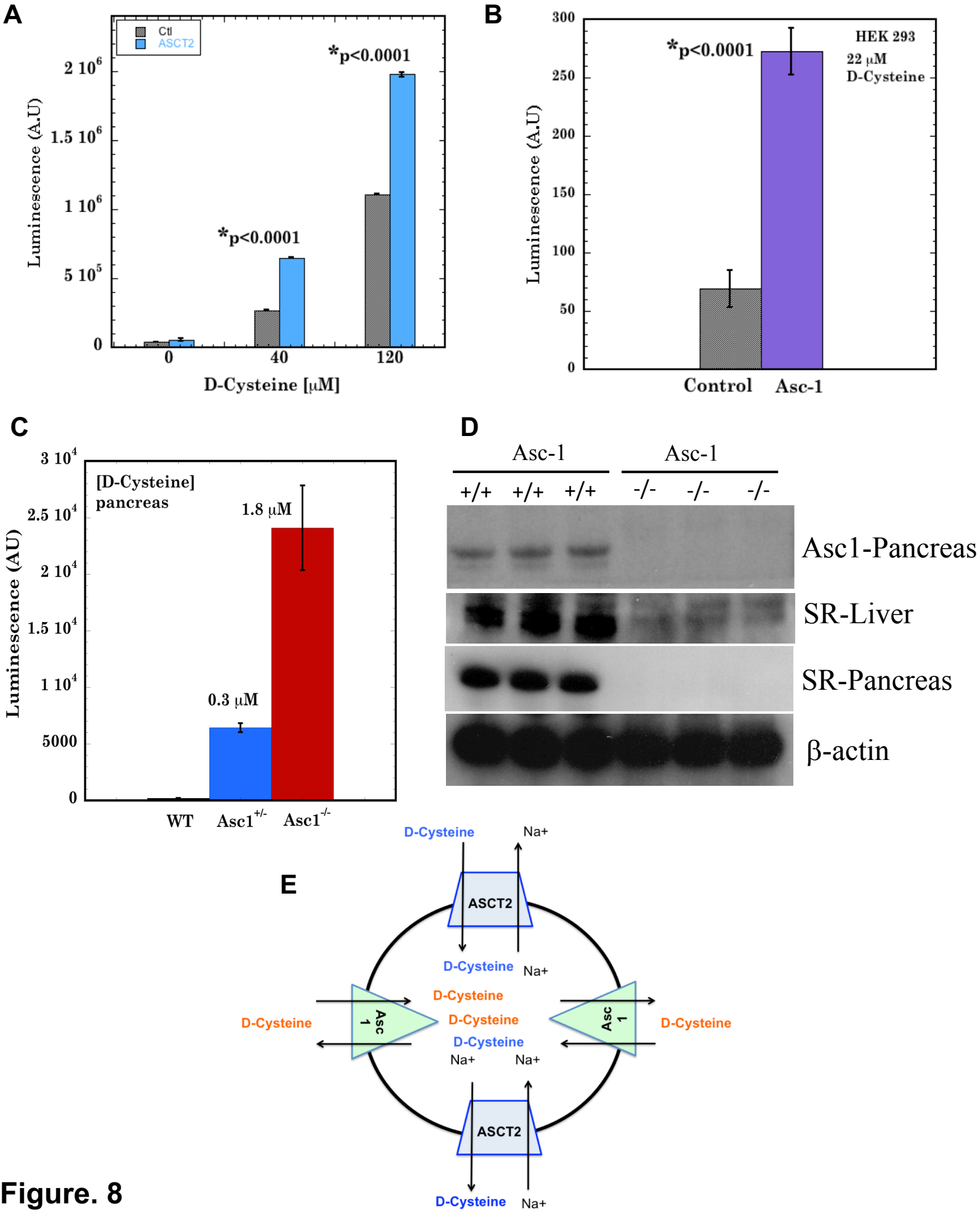
A
Ctl
ASCT2
*p<0.0001
*p<0.0001
Luminescence (A.U)
2 10^6
1.5 10^6
1 10^6
5 10^5
0
0
40
120
D-Cysteine [μM]
B
*p<0.0001
HEK 293
22 μM
D-Cysteine
Luminescence (A.U)
300
250
200
150
100
50
0
Control
Asc-1
C
[D-Cysteine]
pancreas
1.8 μM
0.3 μM
Luminescence (AU)
3 10^4
2.5 10^4
2 10^4
1.5 10^4
1 10^4
5000
0
WT
Asc1^+/-
Asc1^-/-
D
Asc-1
Asc-1
+/+ +/+ +/+
-/- -/- -/-
Asc1-Pancreas
SR-Liver
SR-Pancreas
β-actin
E
D-Cysteine
Na+
ASCT2
D-Cysteine
Na+
D-Cysteine
D-Cysteine
D-Cysteine
Asc 1
Asc 1
D-Cysteine
D-Cysteine
Na+
Na+
ASCT2
D-Cysteine
Na+

Figure. 8